Journal of Engineering for Gas Turbines and Power
Available online 13 October 2023, GTP-23-1195
DOI:10.1115/1.4063768

Effect of unsteady fan-intake interaction on short intake design

Luca Boscagli *, David MacManus † and Robert Christie ‡
Cranfield University, MK43 0AL, Cranfield, UK

Chris Sheaf§
Rolls-Royce plc, DE24 8BJ, Derby, UK

The next generation of ultra-high bypass ratio civil aero-engines promises notable engine cycle benefits. However, these benefits can be significantly eroded by a possible increase in nacelle weight and drag due to the typical larger fan diameters. More compact nacelles, with shorter intakes, may be required to enable a net reduction in aero-engine fuel burn. The aim of this paper is to assess the influence of the design style of short intakes on the unsteady interaction under crosswind conditions between fan and intake, with a focus on the separation onset and characteristics of the boundary layer within the intake. Three intake designs were assessed and a hierarchical computational fluid dynamics approach was used to determine and quantify primary aerodynamic interactions between the fan and the intake design. Similar to previous findings for a specific intake configuration, both intake flow unsteadiness and the unsteady upstream perturbations from the fan have a detrimental effect on the separation onset for the range of intake designs. The separation of the boundary layer within the intake was shock driven for the three different design styles. The simulations also quantified the unsteady intake flows with an emphasis on the spectral characteristics and engine-order signatures of the flow distortion. Overall, this work showed that is beneficial for the intake boundary layer to delay the diffusion closer to the fan and reduce the pre-shock Mach number to mitigate the adverse unsteady interaction between the fan and the shock.

Nomenclature

AIP	=	Aerodynamic Interface Plane
a	=	Speed of sound $[m/s]$
CFD	=	Computational Fluid Dynamics
D	=	Diameter $[m]$

*Research Fellow, Centre for Propulsion and Thermal Power Engineering, luca.boscagli@cranfield.ac.uk
†Professor in Propulsion Aerodynamics, Centre for Propulsion and Thermal Power Engineering
‡Lecturer in Aerospace Engineering Design, Centre for Propulsion and Thermal Power Engineering
§Installation Aerodynamics Specialist, Installation Aerodynamics, Rolls-Royce plc

Journal of Engineering for Gas Turbines and Power. Received May 25, 2023;
Accepted manuscript posted October 13, 2023. doi:10.1115/1.4063768
Rolls-Royce plc

f = Frequency $[Hz]$

k = Streamwise curvature $[1/m]$

L = Length scale $[m]$

$MFCR$ = MassFlow Capture Ratio $[-]$

P_0, P = Total and static pressure $[Pa]$

R_{gas} = Ideal gas constant $[J/kgK]$

r = Radial coordinate $[m]$

s = Specific entropy $[J/kgK]$

T_0, T = Total and static temperature $[K]$

t = Time scale $[s]$

U, V = Velocity scale $[m/s, kts]$

Greek symbols

α = Swirl angle $[^\circ]$

γ = Specific heats ratio $[-]$

ζ = Entropy function, $= e^{\frac{-(s-s_\infty)}{R_{gas}}}$ $[-]$

ρ = Density $[kg/m^3]$

ϕ = Azimuthal coordinate $[^\circ]$

ω_{fan} = Fan rotational speed $[rad/s]$

Subscripts

bp = blade passing

hi = intake highlight

in = intake

ref = reference

∞ = free-stream

I. Introduction

The next generation of civil turbofan aero-engines is likely to have a further increase in bypass ratio to reduce the specific thrust and increase the propulsive efficiency. However, the associated typical increase in fan diameter could adversely affect nacelle weight and drag. A net reduction in fuel burn may be accomplished with more compact nacelles [1] and it is envisaged that shorter intakes and exhaust ducts may be used. While a slimmer nacelle will typically enable a reduction in pressure and viscous drag at cruise [2], it may degrade the boundaries for intake boundary layer separation at take-off and climb-out conditions [3] with a consequent reduction in intake-fan compatibility range. An important

Journal of Engineering for Gas Turbines and Power. Received May 25, 2023;
Accepted manuscript posted October 13, 2023. doi:10.1115/1.4063768
Rolls-Royce plc

operating condition is when the aircraft operates at a high-power static condition on the ground with a crosswind flow. Engine performance and behavior are strongly dependent on the intake design and the ability to deliver low levels of flow distortions [3]. For an isolated engine which operates near the ground there are mainly two mechanisms of flow distortion generation; intake lip separation and ground vortex ingestion [4]. Shorter intakes require an increased diffusion capability for a given throat Mach number compared to longer intakes. Thus, the crosswind condition is one of the key drivers for the intake design along with high incidence condition which is typically experienced during second-segment climb [5]. Under crosswind conditions the flow regime within the intake can be considerably different depending on engine mass flow ($\dot{m}$), wind velocity (V_{wind}) and non dimensional ground clearance (H/D_{hi}). Under relatively high mass flow conditions the intake lip flow is transonic and characterized by a near-normal Shock-wave Boundary Layer Interaction (SBLI) (Fig. 1). A further increase in either $\dot{m}$ (or V_{wind}) may lead to shock induced separation with a concomitant increase in flow distortion at the fan face. Moreover, for sufficiently large captured streamtube, a ground vortex is ingested into the engine [6, 7]. In this work the separation characteristics of the boundary layer within a short intake with fan interaction are analysed for the transonic flow regime.

Typically it is possible to avoid over-acceleration of the flow on the intake lip through an increase in the radius of curvature at the intake highlight and a thicker lip profile [4, 8]. However, for a shorter intake this may lead to an increase in diffuser angle which requires an improvement in the diffusion capability of the intake to avoid boundary layer separation. For the crosswind condition the transonic interaction of the flow at the tip of the fan blade may also be adversely affected by the total pressure and swirl distortions introduced by the ground vortex and lead to a notable drop in fan stall margin [9]. Thus, from the intake design point of view the prediction of separation onset of the boundary layer is of primary importance as well as whether the separation mechanism is driven by the intake lip or diffuser design.

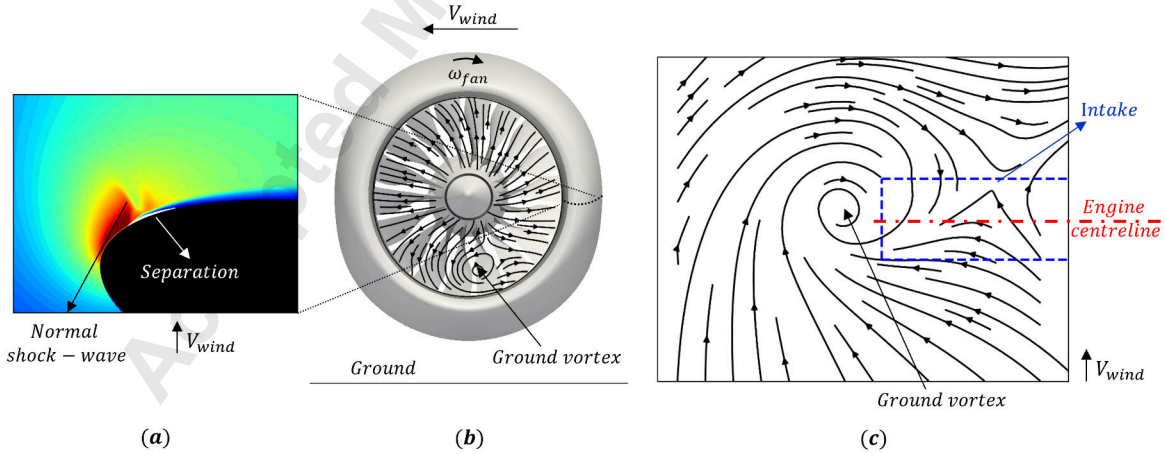

Fig. 1 Schematic of crosswind condition of interest. (a) Shock-wave boundary layer interaction on the intake lip; (b) in-plane streamlines in front of the fan and schematic of the direction of rotation of the ground vortex relative to the fan rotational speed; (c) flow topology on a plane parallel to the ground underneath the intake

Journal of Engineering for Gas Turbines and Power. Received May 25, 2023;
Accepted manuscript posted October 13, 2023. doi:10.1115/1.4063768
Rolls-Royce plc

Peters [5] developed a CFD methodology for short intake design within an industrial context which accounts for the presence of the fan through a body force model. The ratio between the intake length (L_{in}) and fan diameter (D_{fan}) ranged between 0.5 to 0.19 and the impact on overall propulsive efficiency was evaluated. The analyses included a high angle of attack condition and a lower limit of the viable design space of $L_{in}/D_{fan} = 0.25$ was identified due to an increase in Mach number and radial distortion of the total pressure at the fan face. Consequently the notable reduction in fan efficiency and fan operability range for $L_{in}/D_{fan} < 0.25$ out-weighted the reduction in nacelle drag at cruise and resulted in a penalty in the overall propulsive efficiency. Wakelam et al. [10, 11] experimentally investigated two different crosswind regimes within a quasi-3D rig with no ground vortex and no fan-intake interaction. For the transonic regime [11] the flow within the sector rig was either attached or grossly separated from the leading edge of the intake lip. The separation was thought to be associated with SBLI although causality could not be established. The pre-shock Mach number on the intake lip at the pre-separation condition was about 1.35. Steady computational analysis of an intake in crosswind with no ground and no fan [12] showed that a quasi-3D representation of the intake flow may be good enough to capture the separation onset but it was not adequate at post-separation conditions due to the notable changes in the capture streamtube. Nichols et al. [13, 14] experimentally assessed within a low-speed wind tunnel the sensitivity of flow topology within an intake with no fan and no ground in crosswind conditions to changes in either crosswind velocity or engine mass flow rate. The flow on the intake lip was transonic and there was an open separation of the intake boundary layer on the lower windward quadrant that extended to the nominal fan face location. Changes in the intake flow topology relative to a change in either V_{wind} or $\dot{m}$ were established but it was not possible to quantify the sensitivity of the flow separation onset to changes in operating conditions. Recent steady [15, 16] and unsteady [17] CFD studies of short and conventional intakes with fan-coupling under high-incidence conditions showed the impact of intake design style and compactness on the onset of large total pressure and swirl distortions at the fan face due to notable separation of the intake boundary layer. Silva et al. [18] assessed with steady CFD analyses different short intake designs under both high-incidence and crosswind conditions, and evaluated the impact of a change in short intake design on the status of the intake boundary layer. The crosswind analyses were conducted at a single operating point and therefore the separation mechanisms were not fully determined.

Experimental and computational investigations of a cylindrical intake in near ground operations revealed the influence of crosswind velocity, ground clearance and approaching boundary layer profile on the characteristics of the ground vortex [4, 7, 19, 20]. Under crosswind conditions the ground vortex strength is mainly a function of the non dimensional ground clearance (H/D_{hi}) and the ratio between the velocity at the intake highlight plane and the crosswind velocity ($U^* = U_{hi}/V_{wind}$). A ground vortex produces velocity distortions at the fan face along with total pressure loss in the core region [21]. Recent computational analysis of an isolated modern turbofan demonstrator showed an 8% reduction in fan stall margin due to ground vortex like distortions compared to a case where the fan operates with homogeneous flow [9]. Steady and unsteady distortions were assessed and it was found that the low

Journal of Engineering for Gas Turbines and Power. Received May 25, 2023;
Accepted manuscript posted October 13, 2023. doi:10.1115/1.4063768
Rolls-Royce plc

frequency content associated with the fluctuations of the radius of the core of the ground vortex core was detrimental for the fan operability range. The coupled interaction between the intake and the fan with the presence of the ground was experimentally investigated by Freeman and Rowe [22]. The analysis showed that in crosswind conditions the intake flow may exhibit an oscillatory behavior which can lead to premature fan stall. Computational analysis of a fan-intake coupled configuration under crosswind conditions showed that when the ground vortex is not taken into account then the fan is more tolerant to intake total pressure distortions when the fan rotational speed is increased [23]. Computational analysis showed that for a short intake a strong coupled interaction with the fan may be expected at both high incidence [24] and crosswind conditions [25]. For the high incidence conditions, the fan design may be tailored to improve the fan performances when the intake flow is separated and non homogeneous at the fan face [26]. Under crosswind conditions, the impact of fan unsteadiness can augment the amplitude of the axial pulsation for a transonic SBLI which adversely affects the separation onset of the intake boundary layer [25]. Nevertheless, the impact of a change in intake design on the unsteady interaction with the fan was not determined and therefore this is addressed in this work.

For a short-intake there is currently no evidence in the literature on how a change in intake design affects the intake flow separation mechanisms and the unsteady interaction with the fan under crosswind conditions. Within this context, the aim of this work is to assess the characteristics of fan-intake interactions for a range of intake designs. Three short intake designs were used as test cases to investigate the fan-intake unsteady interactions. A hierarchical CFD approach was used to decouple the contribution of intake flow unsteadiness and fan unsteadiness on the intake critical conditions. The study highlights how the fan-intake interaction in crosswind is affected by a change in intake design and the consequences for short intake design decisions are discussed.

II. Methodology

A. Computational methods

A 3D unstructured finite volume solver (HYDRA,[27]) was used within this work. The numerical fluxes were computed through an approximate Riemann solver of Roe based on a second-order MUSCL scheme for the spatial discretization and a Green-Gauss method was used for the evaluation of the gradients. An implicit second order backward difference scheme [28] was used for the temporal advancement. Reynolds Averaged Navier Stokes (RANS) equations with Spalart-Allmaras (SA) as turbulence closure model were solved within this work. The turbulent production term in SA was based on vorticity and strain [29]. A low Mach number preconditioning technique was used to damp the acoustic modes and improve the initial convergence [30].

A hierarchy of numerical fan models was used within this work. A low order fan model, called the Immersed

Journal of Engineering for Gas Turbines and Power. Received May 25, 2023;
Accepted manuscript posted October 13, 2023. doi:10.1115/1.4063768
Rolls-Royce plc

Boundary Method for Smeared Geometries method (IBMSG, [31]), was used to assess the intake design process, as the intake design space is highly dimensional and it requires a significant amount of computational resources [5]. The IBMSG model assumes that a rotating fan can be modelled through an infinite number of 'zero-thickness' blades. However, both the geometric blockage due to the presence of the fan blades and the aerodynamic blockage due to the growth of the boundary layer in the blade passage are accounted for through a blockage factor that modifies the flow-through area [32]. The force exchanged between the flow and the fan is decomposed into parallel and normal components to the blade camber line and circumferentially averaged within every cell in the region bounded by the blades. The IBMSG model was previously applied to intake at high incidence for both attached and separated cases [33] and also to a short intake in crosswind [25]. Due to the assumption of an infinite number of blades, the IBMSG model is not capable of reproducing the upstream unsteady changes in the static pressure field due to the rotation of the fan blades. Steady and unsteady RANS with IBMSG (RANS-IBMSG and URANS-IBMSG, respectively) can be used to quantify the effect of the intake flow unsteadiness on the separation onset and the characteristics of the boundary layer within a powered intake.

Numerical analyses that models the presence of the fan blades and their temporal variation within the computational domain are also needed to account for the azimuthal variation in the static pressure field within the intake domain upstream of the fan blades. For a typical stage calculation with rotating and stationary components, an internal boundary condition must be specified at the interface between the different turbomachinery components. A steady Mixing-Plane (MP) boundary condition is typically applied for fan design when only single blade passage components without inlet flow distortions are considered. When the latter are taken into account then unsteady full-annulus computations are required to capture both the change in relative reference of frame and the correct temporal variation of the position of the blade row within the flow. Thus, a sliding plane boundary condition is used along with unsteady RANS models (Fig. 2). The adjacent sub-domains are extruded in the direction normal to the interface. This results in a one cell row overlap across the boundaries [28]. The unsteady sliding-plane computations are referred in the following sections as URANS Time Resolved Fan (URANS-TRF) analyses. As the URANS-TRF model does take into account upstream azimuthal changes in the static pressure field due to the rotating fan blades, the comparison between URANS-TRF and URANS-IBMSG provides a quantification of the effect of fan unsteadiness on the separation onset and the characteristics of the boundary layer within the intake. For all the unsteady analyses the computational time-step for the initial transient is set to 10 time-steps per blade passing time (t_{bp}). After 6 fan revolutions, the computational time-step is reduced to ensure 60 time-steps per t_{bp}. The choice of the computational timestep was based on previous work on fan-intake interaction studies under high-incidence and crosswind conditions [24, 34, 35]. Data are sampled at about 5 times the blade passing frequency (f_{bp}) for about 6 fan revolutions which are included in the analysis.

Journal of Engineering for Gas Turbines and Power. Received May 25, 2023;
Accepted manuscript posted October 13, 2023. doi:10.1115/1.4063768
Rolls-Royce plc

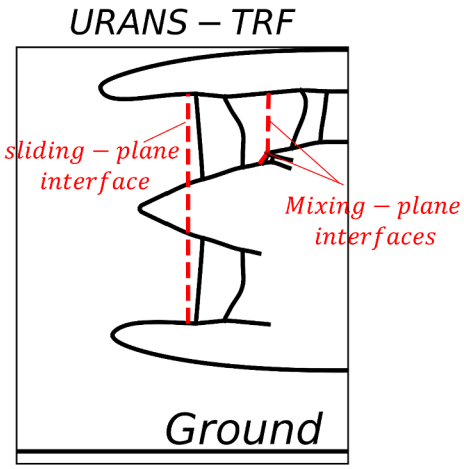

Fig. 2 Schematic of fan-intake interfaces for the unsteady time resolved fan (URANS-TRF) analyses

1. Grid independence studies

Grid independence studies were independently carried out for the intake and the turbomachinery components [25]. For the intake, a grid independence study was carried out based on three levels of mesh refinement which encompassed 6.8×10^6, 10.8×10^6, 35.2×10^6 nodes. The grids were referred to as level 1, 2 and 3. The Grid Convergence Index (GCI) was computed at attached flow conditions. Level 2 grid was sufficiently grid independent with a GCI compared to level 3 grid of 0.014% and 5.6% when applied to IPR and DC60 respectively. A spatial discretization error was also quantified based on the isentropic Mach (M_{ise}) evaluated on the intake surface,

$$M_{ise} = \sqrt{\frac{2}{\gamma - 1}\left[\left(\frac{P_{0,\infty}}{P}\right)^{\frac{\gamma-1}{\gamma}} - 1\right]} \tag{1}$$

A GCI was computed based on the peak M_{ise} on the windward side of the intake, at an azimuthal position (ϕ) 90° from the top dead centre. Level 2 grid had a GCI compared to level 3 grid of 0.67%.

For the turbomachinery components, single passage steady RANS with mixing-plane boundary conditions were used to assess grid sensitivity. Three different levels of grid refinement were generated whose overall size was 4.4×10^6, 8.2×10^6 and 16.2×10^6 nodes. The grids are referred to as level 1, 2 and 3, respectively, and the GCI was evaluated at the fan peak efficiency point. Level 1 grid was considered sufficiently grid independent with a GCI with respect to level 2 grid of 0.04% and 0.035% when applied to RTPR and η_{ad} respectively.

Journal of Engineering for Gas Turbines and Power. Received May 25, 2023;
Accepted manuscript posted October 13, 2023. doi:10.1115/1.4063768
Rolls-Royce plc

2. CFD methods validation and verification

For the intake calculations, the computational methods were previously validated through an analysis of a non-axisymmetric intake geometry with no ground plane and no fan [25]. The comparison between experiments and CFD was based on a total pressure distortions metric (DC60) at an Aerodynamic Interface Plane (AIP). The Mass Flow Capture Ratio (MFCR) where DC60 exceeded the typical threshold was referred to as a critical MFCR ($MFCR_c$). The difference with the experimental data was quantified based on the prediction of the $MFCR_c$,

$$\Delta MFCR_c[\%] = \frac{MFCR_{c,CFD} - MFCR_{c,WTT}}{MFCR_{c,WTT}} 100 \tag{2}$$

where $MFCR_{c,CFD}$ and $MFCR_{c,WTT}$ are the prediction of critical MFCR from the CFD and from the experiment respectively. Overall steady RANS analyses could predict the critical MFCR with $\Delta MFCR_c \approx 6\%$ at the high-speed crosswind regime (Fig. 3). The effect of intake unsteadiness on the critical MFCR was also quantified through unsteady RANS (URANS). The URANS model confirmed the steady prediction of the critical MFCR with a discrepancy relative to the RANS prediction of about ±1-2%.

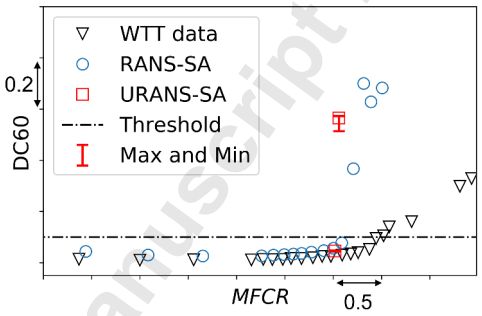

Fig. 3 Effect of MFCR on DC60 for the high-speed (transonic) crosswind regime. Comparison of steady and unsteady RANS computations with Wind Tunnel Test (WTT) data. Figure adapted with permission from Boscagli et al. [25]

For the turbomachinery calculations, steady single-stage (RANS with mixing-plane) and unsteady full-annulus (URANS with sliding-plane) computations were previously [25] validated with experimental data for the same rotor and stator blade geometries used for the fan-intake studies in the results section. The test case included the rotor and stator sections for a low-pressure compression system with no intake geometry and flow distortions. The range of non-dimensional flow function and fan speed investigated included the operating point that is representative of the intake coupled system under crosswind conditions.. The comparison between CFD and experiments was based on Rotor Total Pressure Ratio ($RTPR = \frac{\overline{P_{0,fan-outlet}}}{\overline{P_{0,fan-face}}}$) and rotor adiabatic efficiency (η_{ad}) and the agreement between experiments and CFD was quantified (Eq. 3).

Journal of Engineering for Gas Turbines and Power. Received May 25, 2023;
Accepted manuscript posted October 13, 2023. doi:10.1115/1.4063768
Rolls-Royce plc

$$\Delta RTPR = RTPR_{CFD} - RTPR_{EXP}, \quad \Delta\eta_{ad} = \eta_{ad,CFD} - \eta_{ad,EXP} \tag{3}$$

At the nominal non-dimensional flow function and fan rotational speed for the crosswind operating point, $\Delta RTPR$ and $\Delta\eta_{ad}$ were approximately 0.01 and 1.2%, respectively.

The IBMSG model [31], based on different fan blades representative of the low-pressure compression system of a turbofan aero-engine, was validated with experimental data for a transonic rotor with [36] and without [32] inlet flow distortions. In addition, the IBMSG method was also previously evaluated and compared with steady and unsteady CFD results, with mixing-plane and sliding-plane approaches, for a fan-intake coupled analyses at maximum take-off conditions [33, 36]. For the range of conditions and blade geometries investigated, the IBMSG model was able to capture the radial mass flow redistribution upstream of the fan, which is an important consideration for the intake-fan interaction.

Overall, the computational approach was considered acceptable within the context of this work. The accuracy of the methods used cannot be fully determined due to the lack of a complete experimental validation test case for the coupled fan-intake model. Nevertheless, this is out of the scope of this research, which is focused on the analysis of the effect of a change in intake geometry on the separation characteristics of the boundary layer within short intakes with fan interaction.

3. Computational domain and boundary conditions

The computational domain for the short intake analyses encompassed a quarter sphere which incorporates intake, ground plane and fan. The edges of the computational domain were positioned at about $35D_{fan}$ away from the intake which is far enough based on previous work [23, 24]. Static pressure far-field boundary conditions were applied at the freestream. The ground plane, intake, spinner and fan cowl were modelled as viscous walls. The intake operated at sea-level static conditions with fixed engine mass flow to achieve the desired Mach at the fan face. The wind velocity (V_{wind}) was increased until flow separation reached the AIP (critical crosswind speed, $V_{wind,c}$) and $Re_{D_{hi}}$ varied accordingly between 2.8×10^6 and 5.4×10^6. For all the CFD models for $V_{wind} \leq V_{wind,c}$, the area-averaged total pressure at the AIP for the 3 designs was similar with the differences in time-average IPR that were below 0.5%. The fan operated with a transonic blade-tip interaction for all the conditions analysed. Crosswind direction was such that the inlet vortex and the fan were counter-rotating (Fig. 1).

The computational domains for the RANS-IBMSG, URANS-IBMSG and URANS-TRF computations were spatially discretized through a fully structured approach [37, 38]. The grid resolution requirements in terms of axial, radial and azimuthal resolution separately established for the intake and the fan were used for the coupled fan-intake CFD analyses.

Journal of Engineering for Gas Turbines and Power. Received May 25, 2023;
Accepted manuscript posted October 13, 2023. doi:10.1115/1.4063768
Rolls-Royce plc

The steady and unsteady RANS-IBMSG model encompassed one single domain with an overall grid size of about 14×10^6 nodes. The unsteady Time Resolved Fan (TRF) case included the complete fan assembly and one single blade passage for the Outlet Guide Vane (OGV) and one for the Engine Section Stator (ESS) with an overall grid size of 42×10^6 nodes. A mixing plane boundary condition was used at the interface between fan, OGV and ESS. For all three CFD models a $y^+ \approx 1$ near-wall resolution was ensured and the engine mass flow was controlled through a mass flow outlet boundary condition [24].

B. Intake geometric definition and design intent

Intuitive Class Shape Transformation (iCST, [39, 40]) curves were used to define the parameterization of the intake geometry. The class function is composed of a set of Bernstein Polynomials which are suitable for aerodynamic design and in particular nacelle design [39] given their mathematical regularity [41]. A 3D non-axisymmetric intake design can be represented by a set of aerolines at discrete azimuthal locations (Fig. 4a) which are then blended together through another iCST curve where the fundamental shape of the class function is a straight line. Five aerolines were used at $\phi = 0°$, $45°$, $90°$, $135°$ and $180°$ and at each aeroline 6 geometrical constraints were defined along with three more parameters that defined the main size (r_{hi}/r_{fan}, r_{fan}) and aspect ratio (L_{in}/D_{fan}) of the intake (Fig. 4b). r_{hi}/r_{fan} and L_{in}/D_{fan} set the end-points of the intake aerolines and did not contribute to the overall order of the resultant CST curve. Three different design styles were identified for fixed r_{hi}/r_{fan}, r_{max}/r_{fan}, L_{in}/D_{fan}, scarf angle (θ_{scarf}), offset (Δz_{in}) and H/D_{hi}. In addition, the top ($\phi = 0°$) and bottom ($\phi = 180°$) intake aerolines were also kept the same for the three different designs and azimuthally blended to the sideline ($\phi = 90°$) through the upper ($\phi = 45°$) and lower ($\phi = 135°$) control aerolines respectively.

For a short intake under crosswind conditions both shock induced and diffusion induced separation are likely to occur on the intake lip and diffuser, respectively. Thus, the design intent for the three intake design styles (A, B, C) was to evaluate the sensitivities to the two different separation mechanisms (Fig. 5a). Compared to A, design B had a notable reduction in bulk diffuser angle ($\overline{\theta}_{diff}$, Fig. 4b) to achieve a less aggressive adverse pressure gradient but also had a considerably sharper lip profiles to increase the lip loading and the shock strength. On the other hand, design C, relative to A, had a similar axial distribution of curvature along the diffuser section (Fig. 5b) but an increased radius of curvature at the highlight to achieve a smoother acceleration profile and a different topology of SBLI [8].

C. Data analysis

Distortion metrics of the intake flow were computed at an Aerodynamic Interface Plane (AIP) positioned $0.05r_{fan}$ upstream of the blade tip leading edge. Total pressure distortion and loss were quantified based on $DC60$ and total pressure ratio ($P_0/P_{0,\infty}$), respectively. The separation onset of the boundary layer within the intake was evaluated based on the percentage of reverse mass flow relative to the overall mass flow through the AIP ($\dot{m}^-[\%]$) and a critical

Journal of Engineering for Gas Turbines and Power. Received May 25, 2023;
Accepted manuscript posted October 13, 2023. doi:10.1115/1.4063768
Rolls-Royce plc

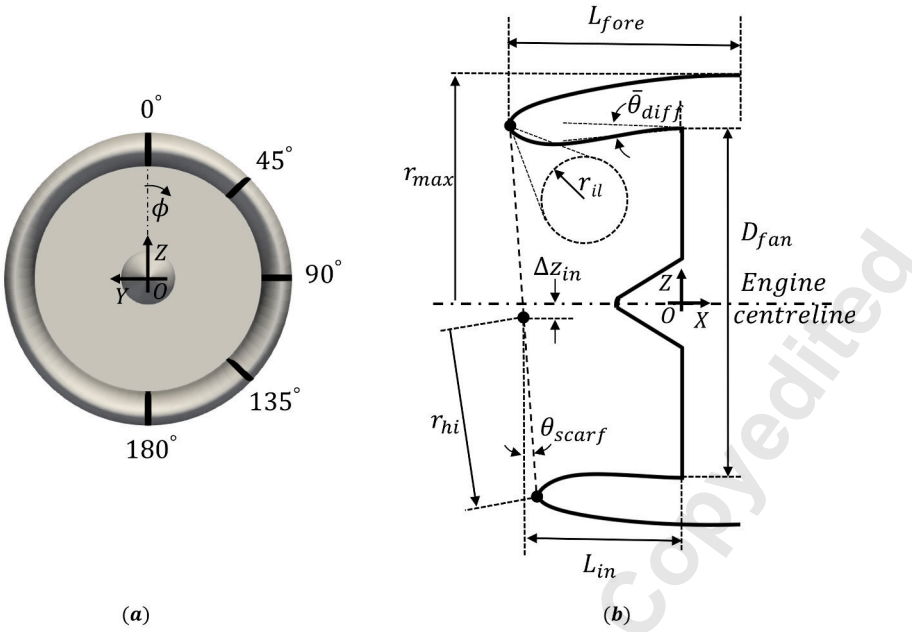

Fig. 4 (a) and (b) schematic of 3D non-axisymmetric intake parameterisation

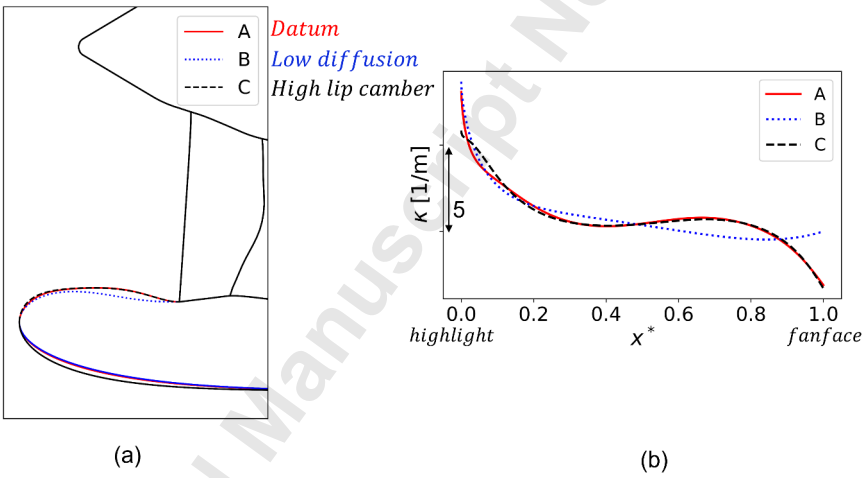

Fig. 5 (a) Intake lip and forebody shape and (b) intake curvature distribution for the three intake designs at $\phi = 90°$

crosswind velocity ($V_{wind,c}$) was established based on $\dot{m}^-[\%] < 0.001\%$. Relative to RANS-IBMSG, URANS-IBMSG computations provide an evaluation of the impact of intake flow unsteadiness on the separation onset and characteristics. When considered within the computational hierarchy, URANS-TRF analyses provide the additional contribution due to the interaction of the fan upstream fluctuations on the unsteady intake flow. The combination of the two effects (intake flow and fan unsteadiness) defines the reduction on the critical crosswind velocity ($V_{wind,c}$) relative to the design method (RANS-IBMSG). For each computational model, the critical crosswind speed ($V_{wind,c}$) of the intake design is evaluated relative to the required reference ($V_{wind,ref}$) crosswind speed (Eq. 4). This defines whether the design requirement is

Journal of Engineering for Gas Turbines and Power. Received May 25, 2023;
Accepted manuscript posted October 13, 2023. doi:10.1115/1.4063768
Rolls-Royce plc

met, and it quantifies the relative margin. This is an important parameter to identify the robustness of an intake design.

$$\Delta V_{wind} = V_{wind,c} - V_{wind,ref} \tag{4}$$

The characteristics of the boundary layer on the intake were determined based on the compressible definition [42] and the outer edge of the boundary layer was determined based on a vorticity magnitude threshold. Typically the outer edge was identified when the vorticity magnitude across the streamwise velocity profile decayed by about three orders of magnitude relative to the value at the wall. Although, downstream of a shock-wave the outer flow field is not strictly irrotational due to the entropy gradient across the shock, the method was sufficiently robust to provide an estimate of the changes in the characteristics of the boundary layer due to a change in intake design and operating conditions.

For the unsteady analysis both the time average quantities and their temporal variation were analysed. A frequency analysis was carried out based on a discrete Fourier transform [43] and the chosen sample frequency dictated a maximum observable frequency within the spectrum of about $2.5f_{bp}$. The spatial distribution of the frequency content was analysed through Banded Fourier spectra [44]. For the URANS-TRF model, in order to evaluate how the signature of the unsteady flow field upstream of the fan is perceived from the rotating fan blades it is important to take into account the relative position of the fan blades within the intake. The post-processing technique was initially used within the context of experimental analyses of complex intake for the characterization of unsteady inlet distortions [45]. Moreover, although at the AIP the flow field is resolved within the absolute reference of frame, relative quantities are computed a posteriori based on a velocity triangle decomposition (Fig. 6).

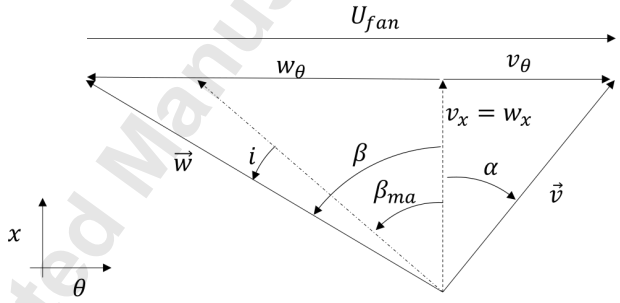

Fig. 6 Velocity triangle at the fan leading edge

The relative velocity vector ($\vec{w}$) in cylindrical coordinates was defined from the absolute velocity vector ($\vec{v}$) and the fan rotational speed U_{fan} as follow

$$\vec{w} = \left(v_r, v_\theta - U_{fan}, v_x\right) = \left(v_r, v_\theta - \omega_{fan} r, v_x\right) \tag{5}$$

where v_r, v_θ and v_x are the radial, tangential and axial absolute velocity vector components respectively. Consequently the relative Mach number (M_{rel}) and relative total pressure ($P_{0,rel}$) can be expressed as

Journal of Engineering for Gas Turbines and Power. Received May 25, 2023;
Accepted manuscript posted October 13, 2023. doi:10.1115/1.4063768
Rolls-Royce plc

$$M_{rel} = \frac{\|\overrightarrow{w}\|}{a} = \frac{\sqrt{v_r^2 + \left(v_\theta - U_{fan}\right)^2 + v_x^2}}{a} \tag{6}$$

$$P_{0,rel} = P\left(1 + \frac{\gamma - 1}{2} M_{rel}^2\right)^{\left(\frac{\gamma}{\gamma - 1}\right)} \tag{7}$$

The blade incidence angle (i) is defined from the relative flow angle (β) and the blade metal angle (β_{ma})

$$i = \beta - \beta_{ma} = \arctan\left(\frac{w_\theta}{w_x}\right) - \beta_{ma} \tag{8}$$

The non dimensional circulation of the core of the ground vortex at the AIP ($\Gamma^* = \Gamma / U_{hi} D_{hi}$) was computed using the vorticity disk method approach [46] where the center of the core of the ground vortex was selected based on the maximum value of signed axial vorticity. The unsteady characteristics of the flow distortions at the AIP were quantified through a discrete Fourier decomposition and banded Fourier spectra were used to identify the spatial distribution of the unsteady fluctuations. For the coupled intake-fan configurations (URANS-TRF) the flow field is characterized by both high frequency and low frequency content [25] associated with the blade-passing (f_{bp}) and the unsteadiness of the shock and the ground vortex ($f < 0.1 f_{bp}$), respectively. To identify the spectral gap between the low and high frequencies, the frequency resolution of each band was $f_{bp}/10$. Within each band, the maximum amplitude of the fluctuations was used to quantify the unsteady content and enable a comparison between different CFD models and operating conditions.

The spatial characteristics (Engine-Order, EO) of the flow distortions at the AIP were evaluated through a spatial Fourier decomposition in the azimuthal direction

$$\hat{i'}(t; k_{n_\theta}) = \sum_{n_\theta=0}^{2\pi} i'(t; k n_\theta) e^{\frac{2\pi j k n_\theta}{N_\theta}} \quad where \quad 0 \le k \le N_\theta \tag{9}$$

Where j is the imaginary unit ($= \sqrt{-1}$), N_θ is the number of points in the azimuthal direction used to sample in space the signal, k_{n_θ} is the discrete wavenumber, i' is the instantaneous azimuthal distribution of blade incidence angle fluctuations at a fixed radial position and $\hat{i'}$ is the array with the associated spatial Fourier coefficients. The Engine-Order (EO) was defined as the non-dimensional discrete wavenumber ($EO = k_{n_\theta}/2\pi$).

D. Statistical convergence of unsteady simulations

For the URANS-IBMSG and URANS-TRF analyses, the statistical convergence for the mass flow at the fan face ($\dot{m}_{fan}$) was monitored. The percentage deviation ($\Delta\dot{m}_{fan}$) from the reference (imposed) mass flow ($\dot{m}_{fan,ref}$) was quantified (Fig 7). The mean percentage deviation was less than 0.15% and 0.05% for the URANS-IBMSG and

Journal of Engineering for Gas Turbines and Power. Received May 25, 2023;
Accepted manuscript posted October 13, 2023. doi:10.1115/1.4063768
Rolls-Royce plc

URANS-TRF, respectively. This is within the convergence tolerance of the steady RANS-IBMSG simulations. The temporal oscillations of the mass flow at the fan face due to instantaneous boundary layer separation within the intake were typically about ±2% of $\dot{m}_{fan,ref}$. This is approximately equivalent to a change in MFCR due to a $\pm 0.7kts$ variation in crosswind speed at a fixed engine mass flow. This was considered acceptable within the context of this work, where the effect of a change in intake operating conditions on the separation of the intake boundary layer is assessed through a $2kts$ step change in crosswind speed.

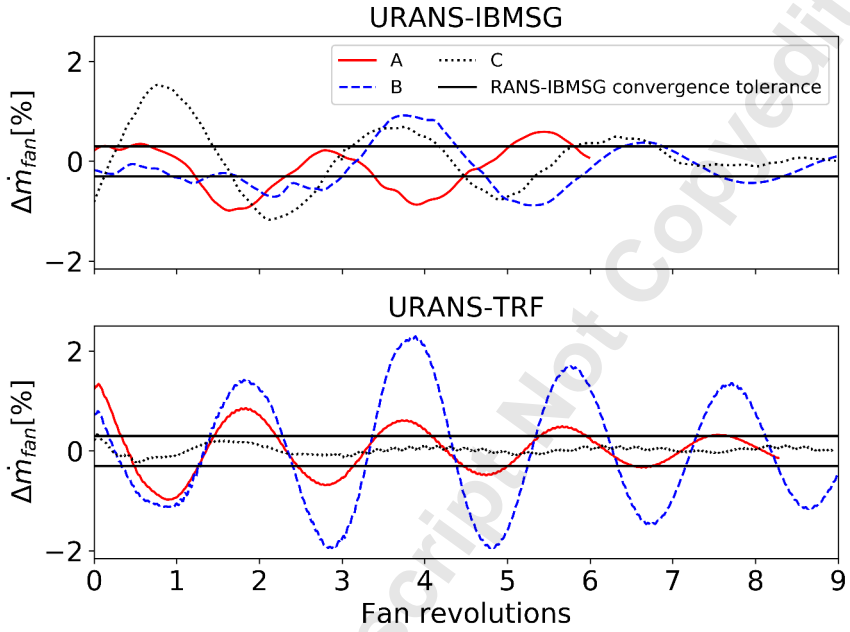

Fig. 7 Time history of percentage deviation of engine mass flow for URANS-IBMSG and URANS-TRF at the critical crosswind speed

III. Results

A. Intake aerodynamic design

A datum short intake (design A) with $L_{in}/D_{fan} = 0.35$ and a ground clearance of $H/D_{hi} \approx 0.45$ was initially defined through a design iteration process that evaluated a range of off-design conditions which included crosswind conditions. The design process used steady RANS with a reduced order model for the fan (IBMSG, [31]) based on state of the art short-intake design [5] practice within an industrial context. Design A met the design requirements ($V_{wind,c} \geq V_{wind,ref}$) with $V_{wind,c} = V_{wind,ref} + 8kts$ (Fig. 8). For the datum design, the total pressure ratio ($P_0/P_{0,\infty}$, Fig. 9a) and swirl (α, Fig. 9b) distributions were significantly non-homogeneous even at the crosswind speed where there was not gross intake boundary layer separation ($V_{wind} - V_{wind,ref} = +2kts$ and $+8kts$). This was due to the presence of the ground vortex in the lower intake quadrant ($\phi \approx 180°$). Positive swirl is defined such that it will tend to

Journal of Engineering for Gas Turbines and Power. Received May 25, 2023;
Accepted manuscript posted October 13, 2023. doi:10.1115/1.4063768
Rolls-Royce plc

reduce the blade incidence angle (i). Thus, the notable negative swirl distortion due to the ground vortex towards the tip of the fan radius tends to increase the blade incidence angle and the strength of the shock on the blade passage [17]. As the crosswind speed significantly increased ($V_{wind} - V_{wind,ref} = +14kts$) there was boundary layer separation on the windward side of the intake, the total pressure at the AIP notably decreased at about $\phi = 90°$ (Fig. 9a) and a region of notable positive and negative swirl also formed (Fig. 9b).

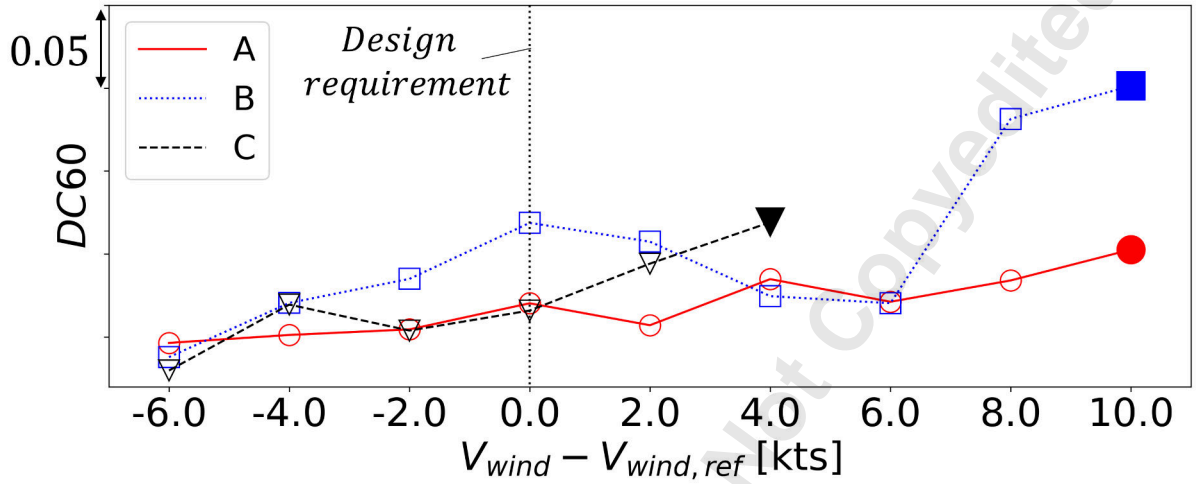

Fig. 8 Effect of increase in crosswind velocity on DC60 at the AIP. Empty symbols (▽): $\dot{m}^-[\%] < 0.001$; filled symbols (▼): $\dot{m}^-[\%] > 0.001$. Critical crosswind speed ($V_{wind,c}$) established based on last attached ($\dot{m}^-[\%] < 0.001$) point. Steady RANS-IBMSG simulations

Two more intakes were designed and referred to as B and C. Based on the design CFD methodology (steady RANS-IBMSG) they both met the design requirements ($V_{wind,c} \geq V_{wind,ref}$) with $V_{wind,c} = V_{wind,ref} + 8kts$ and $V_{wind,c} = V_{wind,ref} + 2kts$ respectively (Fig. 8). The intake design style affected the separation onset of the boundary layer within the intake and therefore a direct comparison at the same crosswind velocity was not useful. Thus, to determine the impact of the intake design style on the separation mechanisms of the intake boundary layer the three intakes were compared relative to their critical condition ($V_{wind,c}$). For design A, the flow at the AIP was attached at $V_{wind,c} = V_{wind,ref} + 8kts$ with an homogeneous total pressure distribution at the AIP (Fig. 10). There was a separation beneath the shock on the intake lip with a closed shock induced separation on the lower quadrant of the windward side of the intake (Fig. 11). An increase in crosswind speed from $V_{wind,c}$ to $V_{wind,c} + 2kts$ led to open separation from the intake lip up to the nominal fan face (Fig. 11).

Design B, compared with A, had a sharper and thinner lip (Fig. 5b) which led to about 0.2 increase in the pre-shock M_{ise} at the $\phi = 90°$ (Fig. 12a). Compared to A, design B had a bulk diffuser angle ($\bar{\theta}_{diff}$, Figure 5b) about 3.5° lower. Within the design intent a lower $\bar{\theta}_{diff}$ was used to mitigate diffusion induced separation. However, the reduced length of the lip for design B compared to A led to a shock sitting closer to the intake throat and to a notable increase in the post-shock diffusion for B compared to A (Fig. 12c). As a result of the adverse interaction, the boundary layer

Journal of Engineering for Gas Turbines and Power. Received May 25, 2023;
Accepted manuscript posted October 13, 2023. doi:10.1115/1.4063768
Rolls-Royce plc

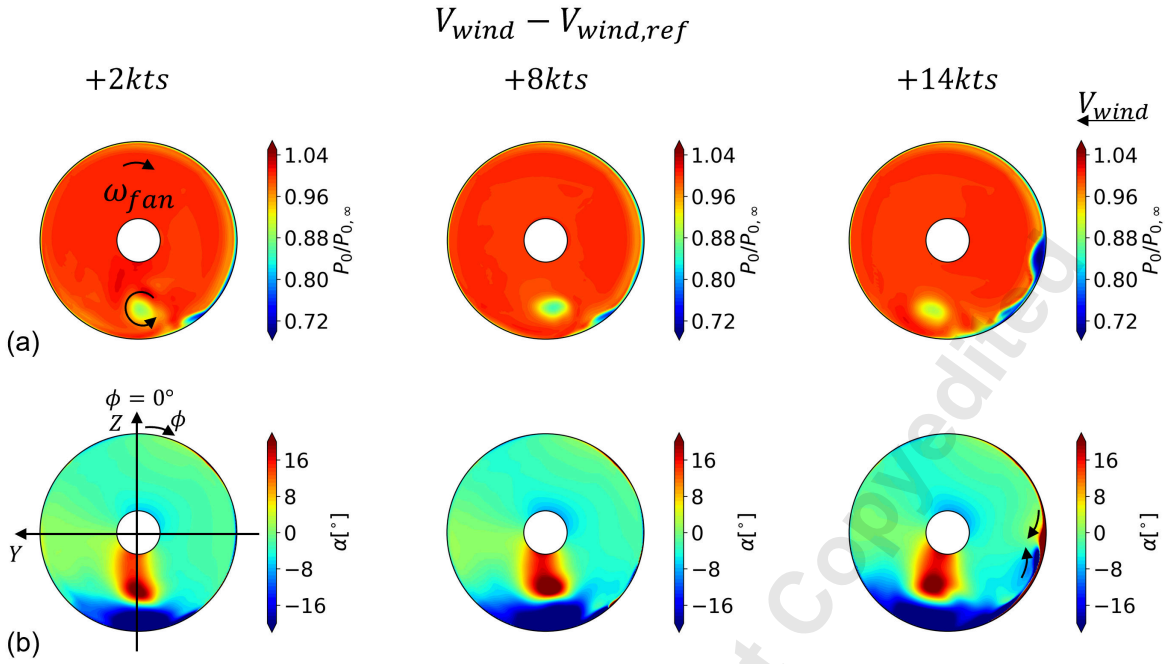

Fig. 9 Effect of increase in crosswind velocity on (a) total pressure ratio ($P_0/P_{0,\infty}$) and (b) swirl (α) distributions at the AIP for design A. Steady RANS-IBMSG simulations

for B was less full relative to A (Fig. 12b) and there was diffusion induced separation on the intake upper quadrant at $V_{wind} = V_{wind,c}$ (Fig. 11). For example, at $\phi = 90°$ at about $x^* = 0.5$ (subplot 2 in Fig. 12b) the compressible momentum thickness of the boundary layer for B was about 50% greater compared to A and the compressible shape factor (H_c) was $H_c = 2.5$ and $H_c = 1.75$ for B and A, respectively.

Compared to design A, design C had a slightly lower bulk diffuser angle (0.4° lower) but a significantly lower rate of change of streamwise curvature on the intake lip ($0 < x^* < 0.1$, Fig. 5b) that led to a more gradual acceleration of the flow over the intake lip region for design C compared to A and about a 0.1 increase in the pre-shock M_{ise} at the $\phi = 90°$ (Fig. 12a). At about the shock location, the local Reynolds number (Re_s) was very similar for A and C at about 3.5×10^6 (subplot 1 in Fig. 12b). The post-throat diffusion for A and C was also very similar in magnitude and delayed to a streamwise location closer to the AIP (Fig. 12c) where the beneficial impact of mass flow redistribution due to the fan plays a more dominant role. Thus, the earlier separation onset of the boundary layer for design C compared to A was primarily associated with the increase in pre-shock Mach number which caused a greater axial and azimuthal extent of shock induced separation at the critical ($V_{wind} = V_{wind,c}$) and post-critical ($V_{wind} = V_{wind,c} + 2kts$) conditions. Thus, there is an indication of the notable importance of the lip design and lip loading for short intake design. This is further explored in the next section where the unsteady flow analyses are presented.

Journal of Engineering for Gas Turbines and Power. Received May 25, 2023;
Accepted manuscript posted October 13, 2023. doi:10.1115/1.4063768
Rolls-Royce plc

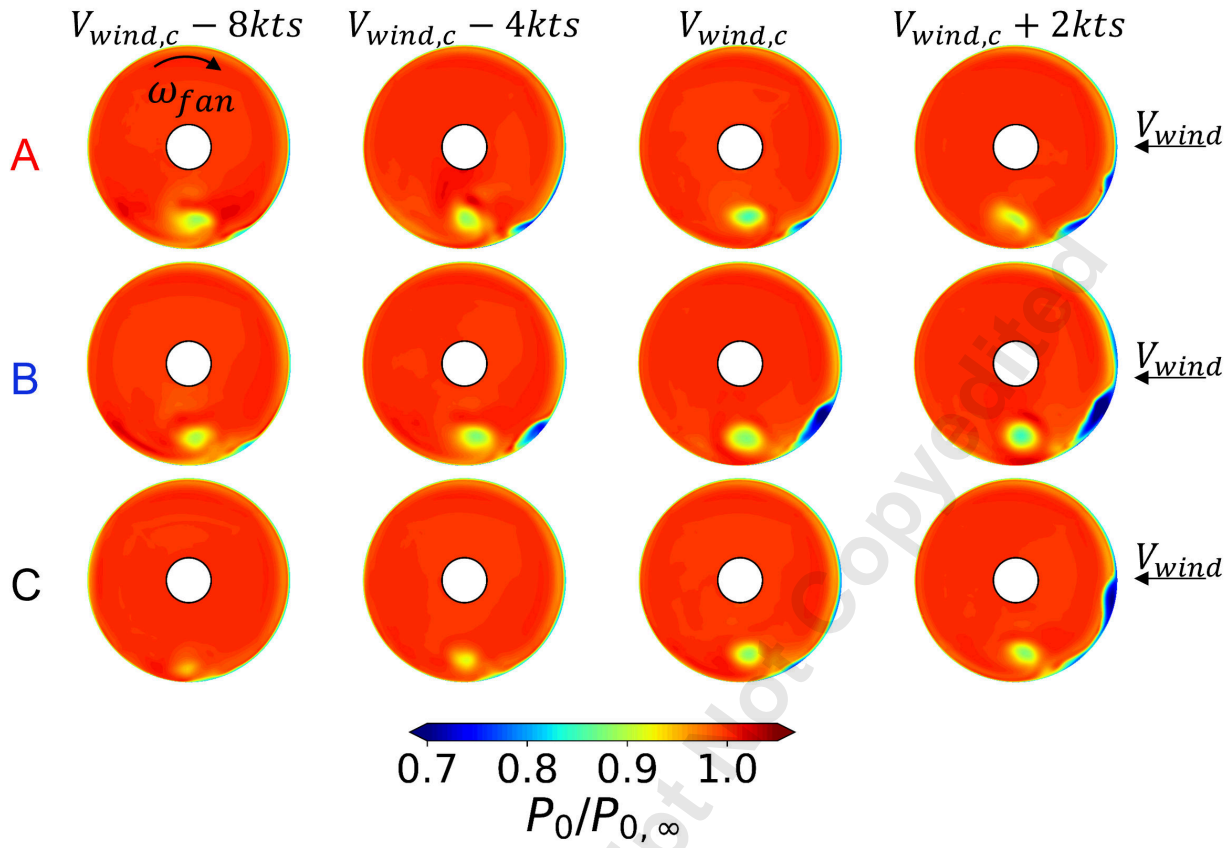

Fig. 10 Effect of increase in crosswind velocity on total pressure ratio ($P_0/P_{0,\infty}$) distribution at the AIP. Steady RANS-IBMSG simulations

B. Unsteady assessment

Although only steady CFD analyses may be viable within a design process, unsteady analyses are required to evaluate the effect of the unsteady features of the intake and fan flow on the prediction of the intake critical conditions [25]. The main objective of this section is to establish the influence of a change in short intake design on the unsteady contributions of intake and fan flow. Compared with the RANS-IBMSG models, the URANS-IBMSG simulations provide an evaluation of the impact of intake flow unsteadiness on the separation characteristics of the intake boundary layer. For all three intake designs (A,B,C), compared with the steady RANS-IBMSG calculations, the critical crosswind velocity ($V_{wind,c}$) was reduced when the intake flow unsteadiness was included with the URANS-IBMSG models. The reduction in $V_{wind,c}$ was $2kts$, $8kts$, $2kts$ for design A, B and C, respectively (Fig. 13). Thus, the impact of intake flow unsteadiness on the intake critical conditions depends on the intake design style.

Compared with the URANS-IBMSG models, URANS-TRF provides an evaluation of the additional effect of fan unsteadiness on the separation onset of the boundary layer within the intake. For all three intake designs the impact of this was a further penalty of a 4 to $6kts$ reduction in $V_{wind,c}$ compared with the URANS-IMBSG calculations (Fig. 13). Based on the full unsteady simulations (URANS-TRF), design A still met the crosswind design requirement

Journal of Engineering for Gas Turbines and Power. Received May 25, 2023;
Accepted manuscript posted October 13, 2023. doi:10.1115/1.4063768
Rolls-Royce plc

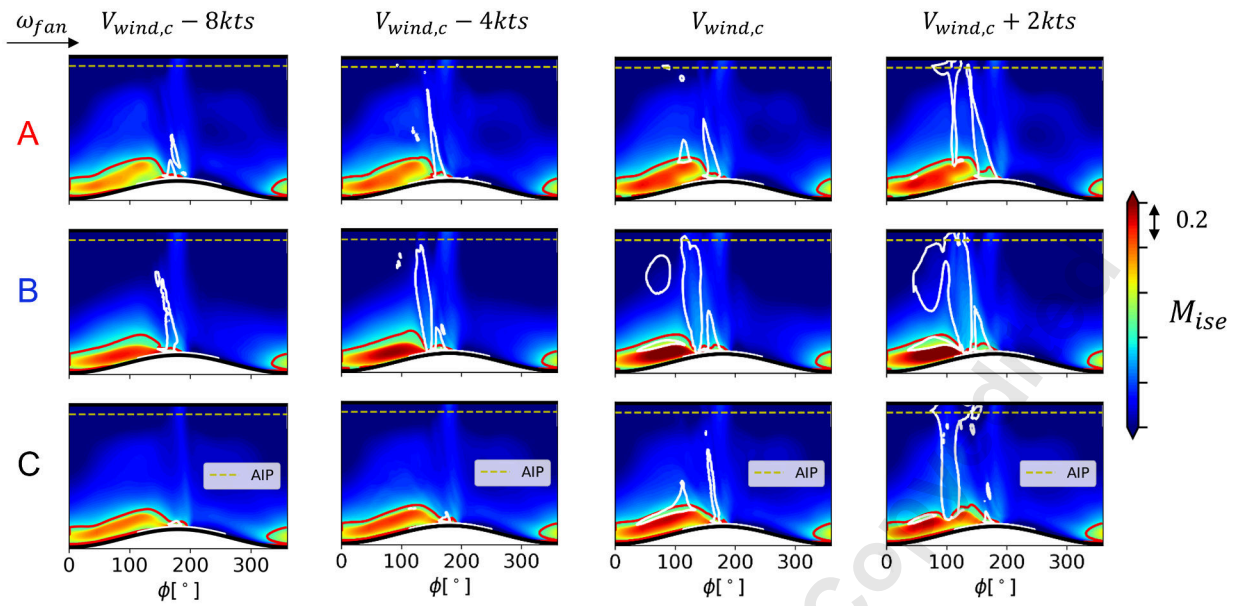

Fig. 11 Effect of increase in crosswind velocity on the isentropic Mach number distribution on the intake surface. Red solid line indicates sonic line ($M_{ise} = 1$); white solid line indicates separation (axial wall shear stress $\tau_{w,x} = 0$). Steady RANS-IBMSG simulations

($V_{wind,c} \geq V_{wind,ref}$) although the design margin ΔV_{wind} was eroded by $6kts$ due to the overall effect of intake flow and fan unsteadiness. On the other hand, design B and C no longer met the acceptability criterion (Fig. 13) when the unsteady fan-intake interaction was taken into account. Overall, based on the URANS-TRF simulations, design A had the best performance with the separation of the intake boundary layer at the AIP that was delayed by approximately $6kts$ and $8kts$ relative to B and C, respectively.

C. Effect of intake flow unsteadiness

The aerodynamic mechanisms that limit the viable design space of short intakes and the characteristics of unsteady flow distortions are determined in this, and the following section, by a comparison of the different designs relative to their critical and post-critical conditions. For the URANS-IBMSG models, banded Fourier spectra of the static pressure fluctuations (p') on the intake surface showed most of the unsteady content within a relatively low frequency band $f/f_{bp} \in [0.01, 0.19]$ (Fig. 14) compared to fan unsteadiness (f_{bp}). At $V_{wind} = V_{wind,c}$, for all 3 designs the main signature was associated with a fluctuation of the axial position of the shock on the intake lip due to the onset of shock-induced separation. As the crosswind velocity was increased, and post-critical ($V_{wind,c} + 2kts$) conditions were approached, the amplitude and axial extent of p' signature across the shock front increased. The three designs had a notable post-throat unsteady content at $V_{wind} = V_{wind,c} + 2kts$ but the main signature was still related to the shock (Fig. 14). Thus, for all the 3 designs, with the URANS-IBMSG simulations, the separation of the boundary layer was shock driven which confirmed previous observations on the influence of the pre-shock Mach number as well as of the axial

Journal of Engineering for Gas Turbines and Power. Received May 25, 2023;
Accepted manuscript posted October 13, 2023. doi:10.1115/1.4063768
Rolls-Royce plc

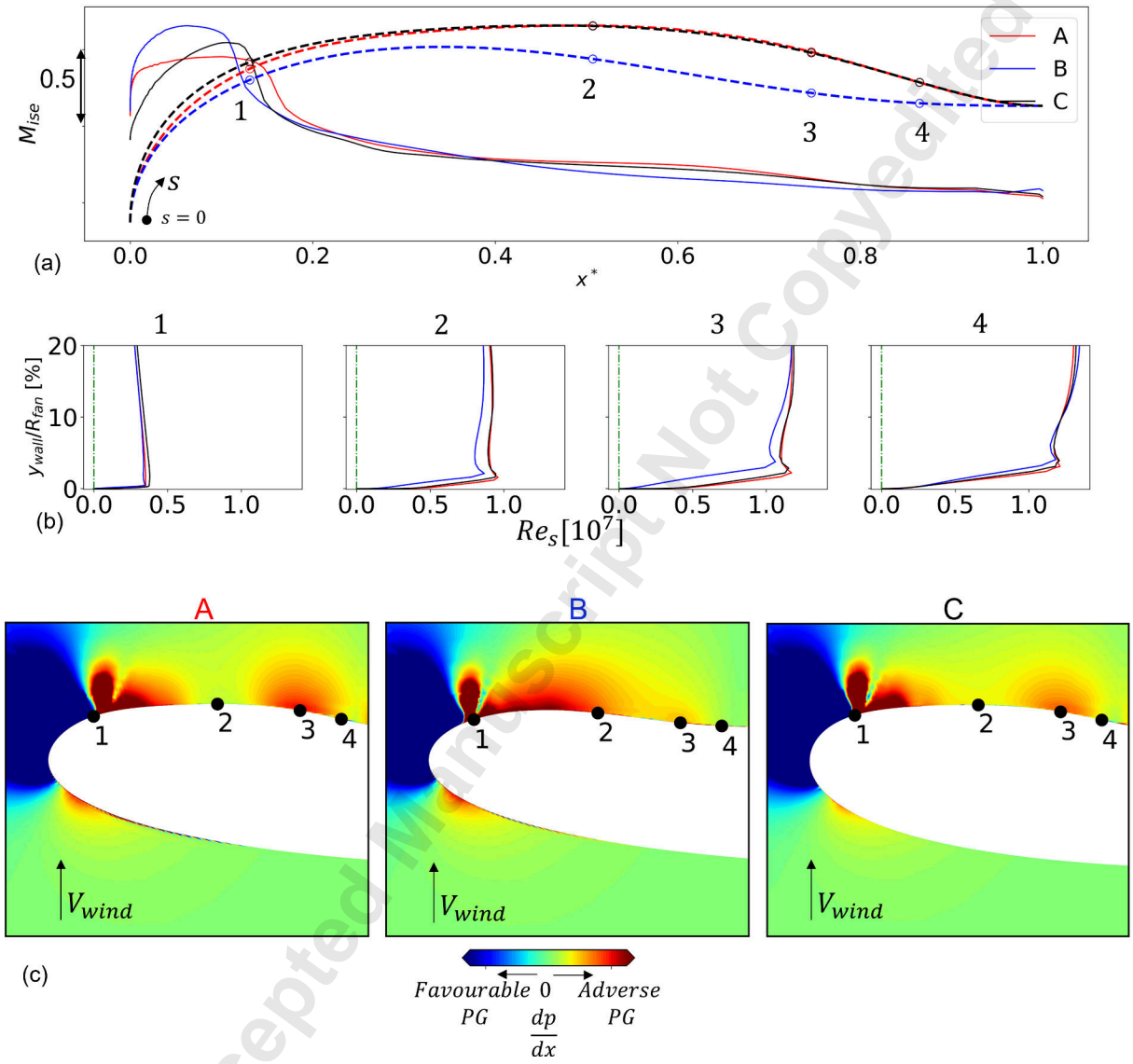

Fig. 12 (a) M_{ise} distribution at the intake sideline, $\phi = 90°$; (b) local Reynolds' number profiles at locations marked in (a); (c) distribution of the axial static pressure gradient on a meridional view at $\phi = 90°$. Steady RANS-IBMSG simulations at $V_{wind} = V_{wind,c}$

Journal of Engineering for Gas Turbines and Power. Received May 25, 2023;
Accepted manuscript posted October 13, 2023. doi:10.1115/1.4063768
Rolls-Royce plc

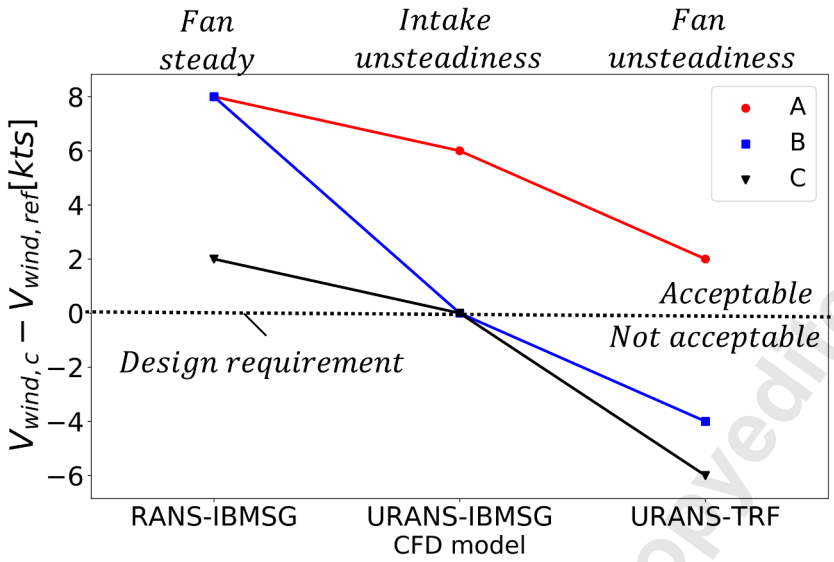

Fig. 13 Influence of intake flow unsteadiness and fan unsteadiness on the critical conditions of the 3 intake designs

position of the shock relative to the intake throat on the separation onset of the boundary layer within a short intake in crosswind. The unsteady characteristics of the flow within the intake at post-critical conditions ($V_{wind} = V_{wind,c} + 2kts$) were broadly independent of the intake design style.

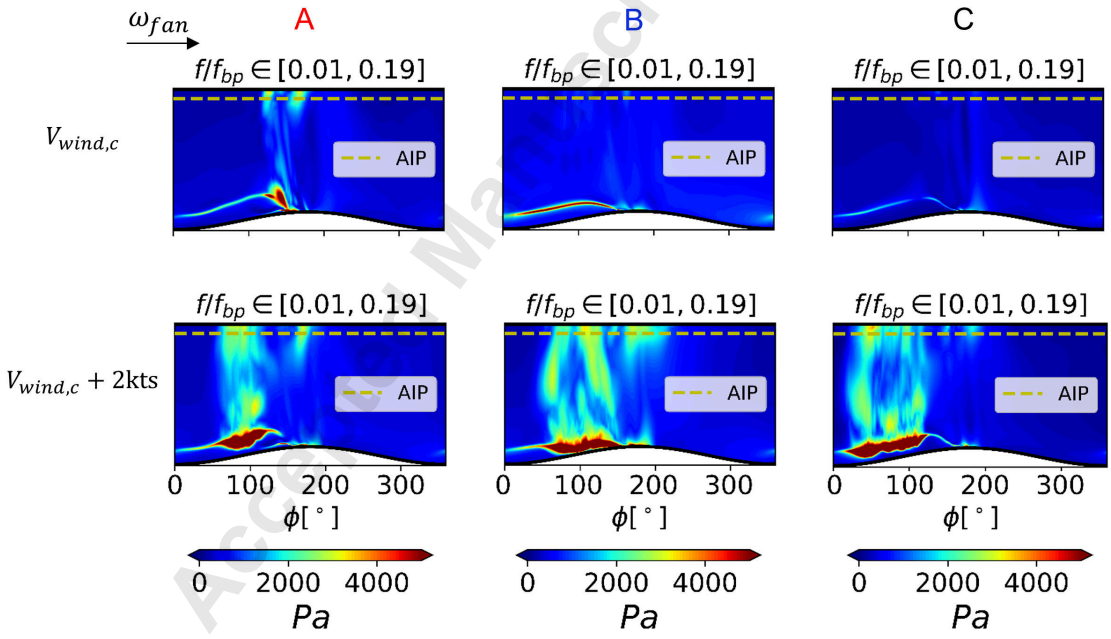

Fig. 14 Spatial distribution of low-frequency static pressure fluctuations on the intake surface at the critical ($V_{wind,c}$) and post-critical ($V_{wind,c} + 2kts$) for the URANS-TRF

Journal of Engineering for Gas Turbines and Power. Received May 25, 2023;
Accepted manuscript posted October 13, 2023. doi:10.1115/1.4063768
Rolls-Royce plc

D. Effect of fan unsteadiness

1. Separation onset and mechanism

For a short intake in crosswind the axial component of the static pressure gradient (dp/dx) had a crucial role in the separation characteristics of the boundary layer. Based on the URANS-TRF simulations at $V_{wind} = V_{wind,c}$, the instantaneous distribution of dp/dx on the intake surface showed a complex flow topology for all three designs (Fig. 15a). On the intake lip the supersonic expansion and the interaction with the shock left a clear signature on the descending blade side ($0° < \phi < 180°$). On the ascending blade side ($180° < \phi < 360°$) the amplitude of fan tip pulsation increased as the fan crossed the ground vortex region ($\phi \approx 150°$, Fig. 15b) and the pressure pulses travelled upstream towards the shock front. The local temporal variation of the static pressure ratio across the shock due to the effect of fan unsteadiness augments the amplitude of the fluctuations of the axial displacement of the shock location [25]. Despite a slightly different propagation angle and initial strength of the fan upstream perturbations, the flow within the three intake designs had similar unsteady characteristics.

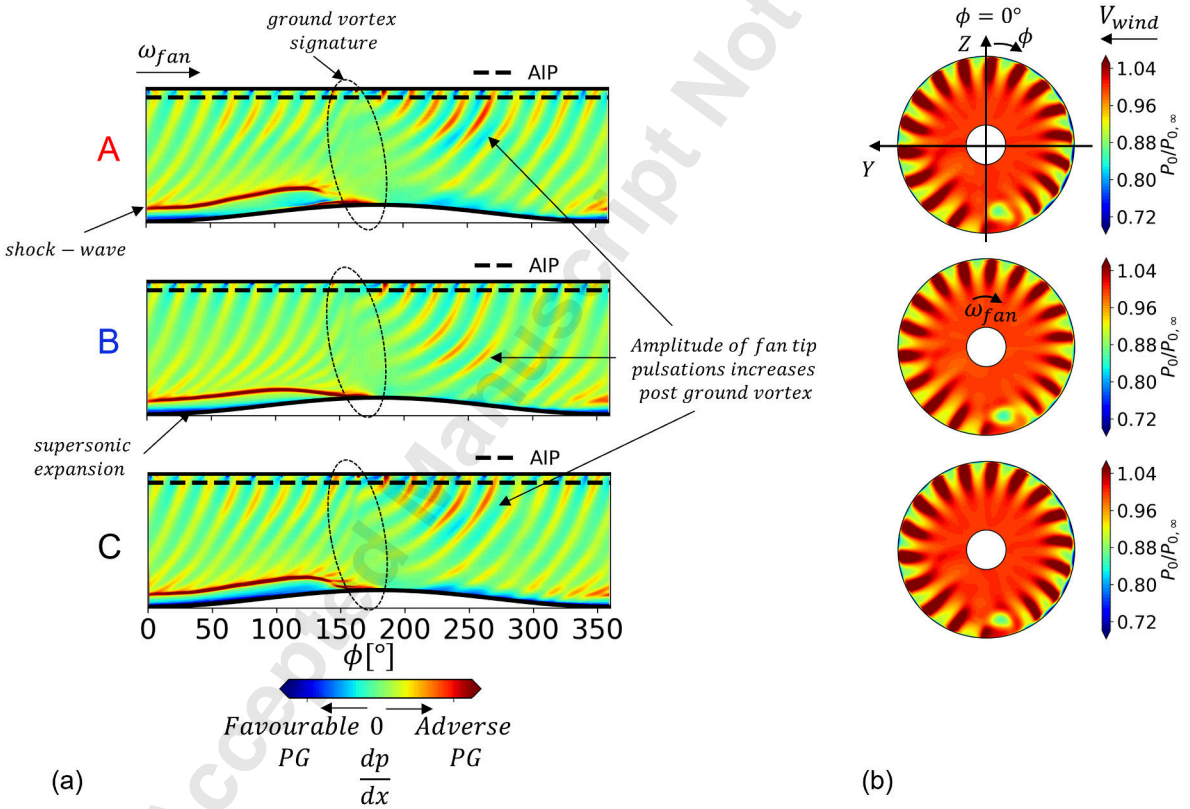

Fig. 15 Time snapshots of (a) axial static pressure gradient on the intake surface and (b) distribution of total pressure ratio at the AIP at the critical crosswind speed ($V_{wind,c}$) for the URANS-TRF simulations

The influence of the different intake design on the decay of the amplitude of fan upstream perturbations was assessed by means of a discrete Fourier transform of the static pressure fluctuations on the intake surface. The decay of

Journal of Engineering for Gas Turbines and Power. Received May 25, 2023;
Accepted manuscript posted October 13, 2023. doi:10.1115/1.4063768
Rolls-Royce plc

blade-passing frequency tone at the intake critical condition ($V_{wind} = V_{wind,c}$) was only slightly different for the three short intake designs. On the windward side ($\phi = 90°$) of the intake the rate of decay suddenly increased upstream of the shock front as the shock-wave typically acts as a low-pass filter [47]. The amplitude of the static pressure fluctuations at a post-shock location ($x^* \approx 0.3$) was about $150dB$ whereas closer to the intake highlight dropped below $120dB$. This indicates that the differences in the intake designs only slightly affected the unsteady interaction between the shock and the fan upstream perturbations and that the impact of fan unsteadiness on unsteady static pressure field within the intake is mostly independent of the intake design style for the range of configurations assessed (Fig. 13).

The reduction in the design margin when fan unsteadiness is taken into account may be explained through an unsteady aerodynamic interaction between the ground vortex, the fan and the shock-wave within the intake. For the investigated combination of fan rotational speed and crosswind direction, both blade tip incidence angle and relative Mach number increase as the fan crosses the ground vortex (Fig. 16a,b, [25]). The tip of the blade ($r/r_{fan} = 95\%$, Fig. 17) is immersed in a region with notable flow distortions for about 0.2 fan revolutions ($\approx 3t_{bp}$). The blade time constant (i.e. the time for a flow particle to travel from the leading edge of the fan blade to the throat of the fan blade channel [48]) at $r/r_{fan} = 95\%$ is approximately $0.6t_{bp}$, so the blade exposure time to ground vortex distortions may reduce the aerodynamic stability limit of the fan as postulated by Cousins [48]. Nevertheless, at $V_{wind,c}$ the distribution of the entropy function downstream of the fan (Fig. 16c) did not show any indication of temporal build-up of fan efficiency losses. The strength of the shock on the suction side of the fan blade increases [17] and so does the amplitude of fan upstream perturbations that reach the shock front on the intake lip (Fig. 15a). Changes in the post-shock static pressure can be perceived upstream of the shock through the boundary layer. The shock must adjust its relative strength to match the new static pressure ratio [49]. As the shock changes its strength and the boundary layer thickens, the shock axial position also changes to remain normal to the local flow direction [50]. The axial position of the shock changes at a relatively low frequency compared to fan unsteadiness ($f/f_{bp} < 0.1$, Fig. 18). The changes in shock strength and axial position subsequently then change the fan inlet flow field through the boundary layer with a notable wideband frequency signature in the Lamb vector modulus [51] which indicates an increase in the interaction of the fan blade with the intake boundary layer. The total pressure loss associated with the boundary layer growth is likely to delay the recovery of the fan blade which will be then exposed to another swirl distortion due to the ground vortex (Fig. 16).

At the critical crosswind speed ($V_{wind,c}$), the three intake designs had notable differences in the amplitude of dp/dx fluctuations at blade-passing frequency (Fig. 18). This was associated with the different velocity ratio ($U^* = U_{hi}/V_{wind}$) at the critical conditions. The ground vortex strength (Γ^*) and core radius (r_c) typically increase with a reduction in U^* [52]. For each individual intake design, both the time average and the amplitude of the fluctuations of Γ^* (Fig. 19a) and r_c (Fig. 19b) were slightly non-monotonic with a change in crosswind speed. Nevertheless, as the 3 designs were compared at the critical crosswind velocity ($V_{wind,c}$) rather than at a fixed crosswind speed, the value of Γ^* at $V_{wind,c}$ monotonically increased from design C to B to A as the values of U^* decreased (Fig. 19a). Thus, the amplitude of the

Journal of Engineering for Gas Turbines and Power. Received May 25, 2023;
Accepted manuscript posted October 13, 2023. doi:10.1115/1.4063768
Rolls-Royce plc

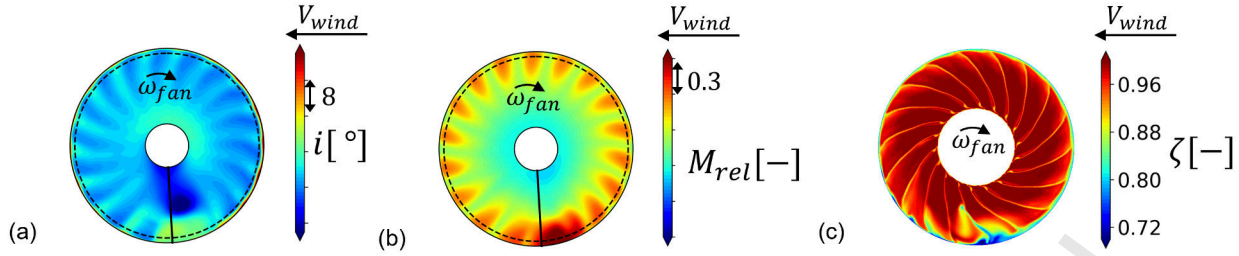

Fig. 16 Time snapshot (after ≈ 3.45 fan revolutions) for design A of (a) blade incidence angle and (b) relative Mach number distributions at the AIP and (c) entropy function at about $0.22r_{fan}$ downstream of the trailing edge of the fan blade tip. The black solid line indicates the approximate azimuthal position of one blade; the dashed line indicates $r/r_{fan} = 95\%$. URANS-TRF simulations at $V_{wind} = V_{wind,c}$

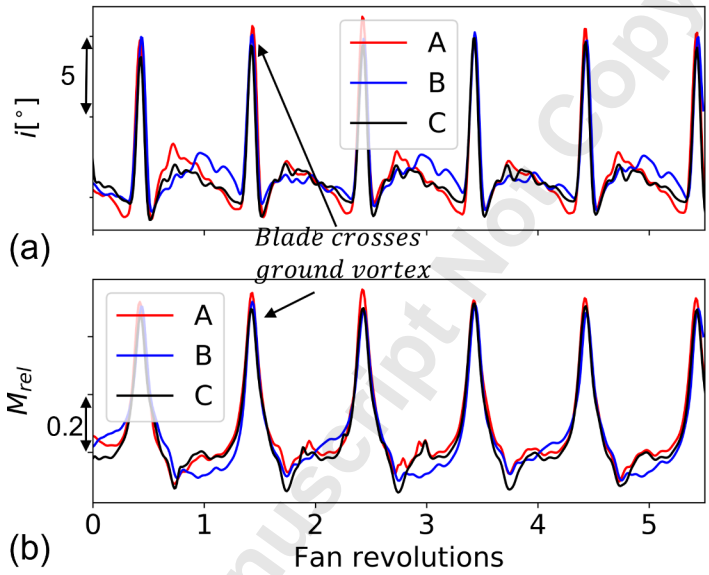

Fig. 17 (a) Blade incidence angle and (b) relative Mach number variation at the tip ($r/r_{fan} = 95\%$) of one blade through 5.5 fan revolutions. URANS-TRF simulations at $V_{wind} = V_{wind,c}$

dp/dx fluctuations increased with the ground vortex strength. This further confirmed the role of the ground vortex on the increase in amplitude in the fan upstream pulsations which have an adverse effect on the separation onset of the boundary layer within the intake.

2. Space-time characteristics of flow distortions

At the post-critical conditions ($V_{wind,c} + 2kts$), the flow field within the intake was unsteady and characterized by both low and high frequency content due to unsteady SBLI and variations in the ground vortex size and strength and blade-passing harmonics respectively. For the three different intake designs the axial displacement of the shock was associated with a frequency signature of $f/f_{bp} \approx 0.03$ (Fig. 20). Closer to the fanface ($x^* = 0.9$), the amplitude of static pressure fluctuations associated with blade-passing was dominant although a low-frequency signature due to the

Journal of Engineering for Gas Turbines and Power. Received May 25, 2023;
Accepted manuscript posted October 13, 2023. doi:10.1115/1.4063768
Rolls-Royce plc

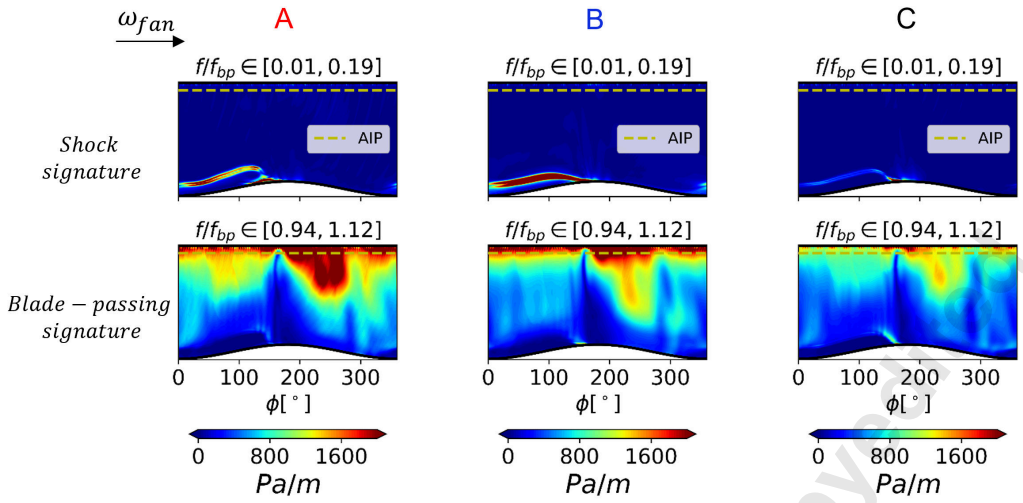

Fig. 18 Banded Fourier spectra of the fluctuations of the axial static pressure gradient on the intake surface. URANS-TRF simulations at $V_{wind} = V_{wind,c}$

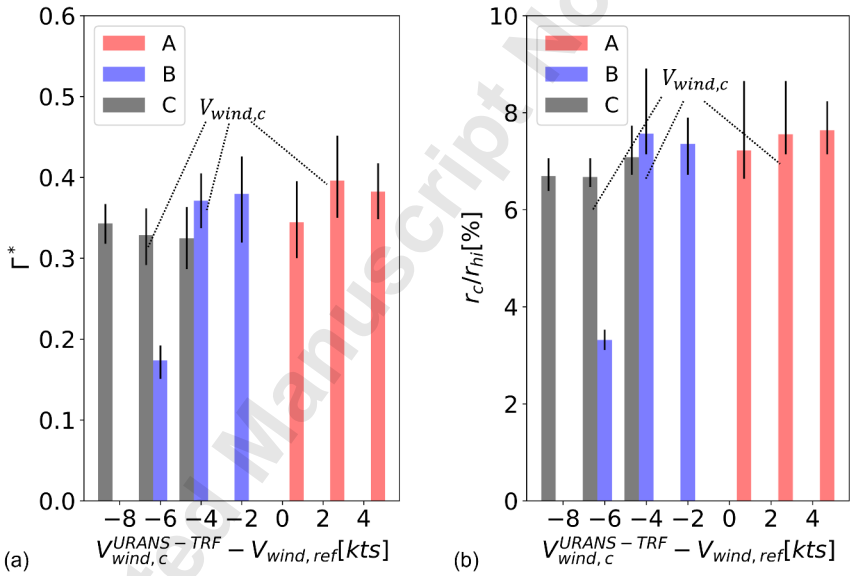

Fig. 19 Time average values (colored solid bars) and fluctuations (black solid range bars) of the non dimensional (a) circulation and (b) radius of the core of the ground vortex at the AIP for the 3 design styles (A, B, C). URANS-TRF simulations

boundary layer separation had similar amplitude to the first blade-passing super-harmonic. On the windward side of the intake ($\phi = 90°$), at about half of the intake length ($x^* = 0.5$), there were two signatures within the spectrum associated to the low frequency content due to intake flow unsteadiness and the higher frequency due to the upstream perturbations from the fan.

The spatial [53, 54] and temporal characteristics of the intake flow distortions are important within the context of the

Journal of Engineering for Gas Turbines and Power. Received May 25, 2023;
Accepted manuscript posted October 13, 2023. doi:10.1115/1.4063768
Rolls-Royce plc

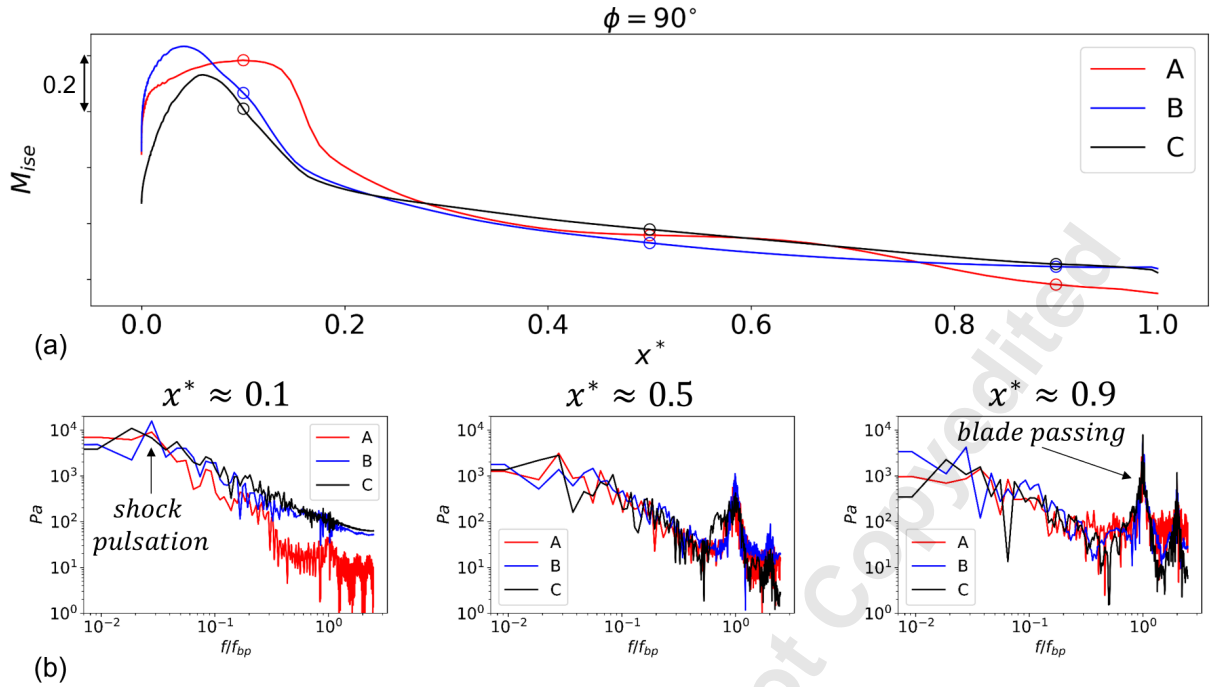

Fig. 20 (a) Time average M_{ise} distribution at $\phi = 90°$ and (b) Fourier analysis of static pressure fluctuations at axial positions marked in (a). Intake A, B, and C at post-critical condition ($V_{wind,c} + 2kts$). URANS-TRF simulations

aero-mechanical response of the compression system, particularly relative to high-cycle fatigue and resonance analysis [55]. This is particularly true for high-loaded fan blades such as those of a low-speed fan [56, 57]. Thus, for a closely coupled fan-intake in crosswind conditions, the influence of intake design on the temporo-spatial characteristics of the intake flow distortions has to be determined. EO spatial characteristics of the time-average blade incidence angle distribution ($\langle \hat{i'} \rangle$) at the AIP showed a very similar radial distribution for the three intake design styles (Fig. 21). The 1EO amplitude was dominant and it was mostly associated with the time-average swirl distortions due to the ground vortex. However, as the flow within the intake was unsteady, the temporal variation of the EO characteristics was also quantified. For the different intake design styles, the temporo-spatial characteristics of the velocity distortions were determined based on the temporal evolution of EO characteristics of the blade incidence angle variations (Fig. 22). For example, the EO characteristics at $r/R_{fan} = 91\%$ for the 3 designs had an almost periodic behavior at about 5EO. The amplitude of the 5EO on blade incidence angle increased to $\approx 3°$ approximately every 2 fan revolutions ($f/f_{bp} \approx 0.03$). This may be associated with the axial pulsation of the shock on the intake lip, which was a common characteristics to all 3 designs at the post-critical crosswind speed ($V_{wind} = V_{wind,c} + 2kts$). Relative to the analysis of the time-average flow field (Fig. 21), the maximum temporal variation of the amplitude of the 3-6EO components of the blade incidence angle (Fig. 22) was about twice as large. The amplitude of the incidence angle distortions at 1EO also increased to about 5°. Compared to A, the amplitude was slightly greater for B despite the 6kts lower crosswind speed. The latter

Journal of Engineering for Gas Turbines and Power. Received May 25, 2023;
Accepted manuscript posted October 13, 2023. doi:10.1115/1.4063768
Rolls-Royce plc

was associated with significantly greater temporal fluctuations of the ground vortex characteristics for B relative to A (Fig. 19) at the post-critical conditions ($V_{wind} = V_{wind,c} + 2kts$). Conversely, the unsteady amplitude of the 1EO characteristics was similar for A and C. Thus, a reduction in bulk diffuser angle and increase in pre-shock Mach number (intake B relative to A) may contributed to an increase in the amplitude of the spatial Fourier coefficients. Relative to the time-average flow field, the unsteadiness of the intake flow field did not significantly affected the amplitude of the 1EO blade incidence angle characteristics. Overall, there was a notable temporal variation of EO characteristics associated with the shock axial displacement at the intake post-critical conditions. Thus, the time-averaged flow distortions may not be sufficient to establish the fan aero-mechanical behavior for given blade modal shapes. However, the radial distribution of the EO characteristics was not considerably affected by a change in intake design style.

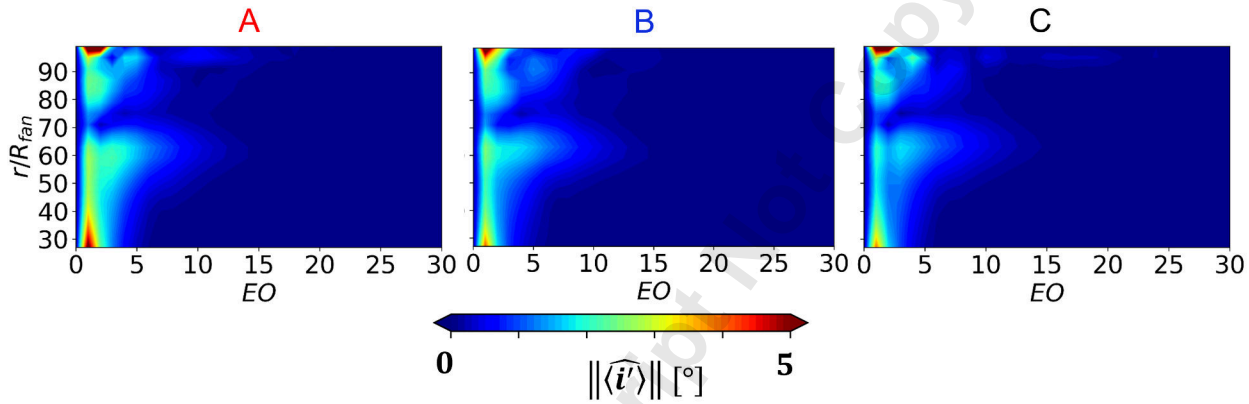

Fig. 21 Spanwise variation of the amplitude of the EO characteristics of the time-average blade incidence angle distribution at the AIP. Intake A, B, and C at post-critical condition ($V_{wind,c} + 2kts$). Time-average URANS-TRF simulations

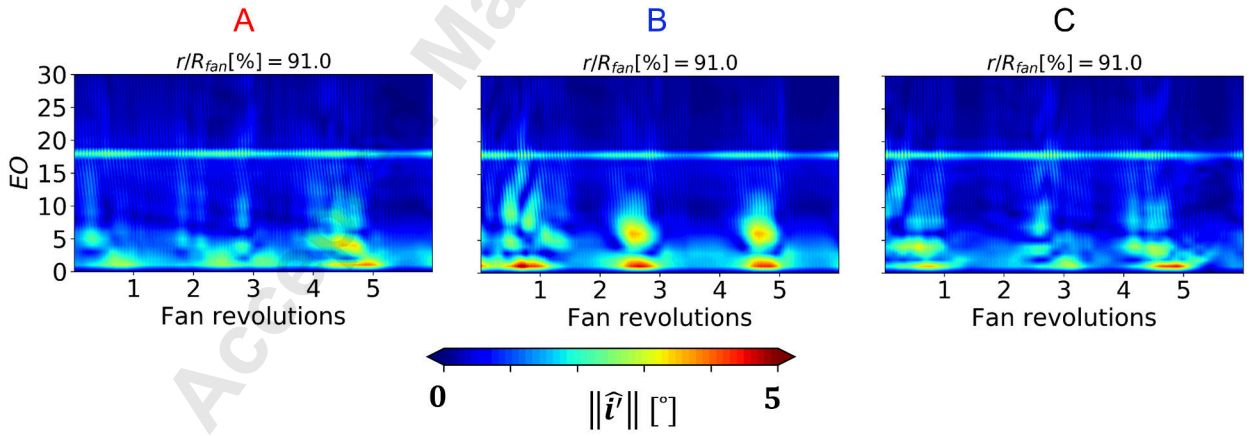

Fig. 22 Temporal variation of EO amplitude of AIP blade incidence angle fluctuations at $r/R_{fan} = 91\%$. Intake A, B, and C at post-critical condition ($V_{wind,c} + 2kts$). URANS-TRF simulations

Journal of Engineering for Gas Turbines and Power. Received May 25, 2023;
Accepted manuscript posted October 13, 2023. doi:10.1115/1.4063768
Rolls-Royce plc

IV. Conclusion

The novel outcome of this work was the assessment of the effect of the short intake design on the unsteady fan-intake interactions under crosswind conditions. The adverse effect of both intake flow and fan unsteadiness on the separation onset and characteristics of the intake boundary layer was quantified for the first time for a range of intake design styles. The main contribution was the identification and evaluation of the key aerodynamic parameters which influence the separation onset of the boundary layer within the intake for a range of designs. These are the strength of the shock, the status of the boundary layer on the lip and the post-shock adverse pressure gradient. From an intake design perspective, this highlights that it is beneficial to delay the diffusion closer to the fan to off-load the lip and avoid premature separation of the boundary layer due to the interaction with the shock. At the post-critical conditions the unsteady characteristics of the shock axial pulsation were almost the same across the different designs and associated to a low frequency signature. When fan unsteadiness was taken into account an unsteady aerodynamic mechanism between the ground vortex, the shock wave on the lip and the upstream perturbations associated with the fan shock was identified which further eroded the crosswind design margin that is required within a design process based on steady RANS with a reduced order fan model. The amplitude of the upstream pulsations from the fan significantly increased due to the interaction between the fan and the swirl distortions associated with the ground vortex. The separation of the intake boundary layer was shock-driven and it was not significantly affected by the intake design style. At the post-critical conditions the space-time characteristics of the intake flow distortions were quantified for the different intake designs. The analysis of the time-average flow field under-predicted the amplitude of the 3-6EO characteristics of the blade incidence angle by about 50%. However, the unsteady EO characteristics of the blade incidence angle were not significantly affected by a change in the intake design style.

Acknowledgments

The doctoral studies of Luca Boscagli were partially funded by Rolls-Royce, plc., and the Engineering and Physical Sciences Research Council (industrial case award 16000032).

Data availability statement

Due to commercial confidentiality agreements the supporting data are not available.

References

[1] Daggett, D., Brown, S., and Kawai, R., "Ultra-Efficient Engine Diameter Study," Tech. Rep. 212309, NASA, 2003.

[2] ESDU, "Mass flow and momentum functions for one-dimensional flow of gas in ducts," *Engineering Sciences Data Unit, Data Items*, , No. 81004, 1981.

[3] Sóbester, A., "Tradeoffs in Jet Inlet Design: A Historical Perspective," *Journal of Aircraft*, Vol. 44, No. 3, 2007, pp. 705–717. https://doi.org/10.2514/1.26830.

[4] Trapp, L. G., and Da Motta Girardi, R., "Crosswind effects on engine inlets: The inlet vortex," *Journal of Aircraft*, Vol. 47, No. 2, 2010, pp. 577–590. https://doi.org/10.2514/1.45743.

[5] Peters, A., Spakovszky, Z. S., Lord, W. K., and Rose, B., "Ultrashort nacelles for low fan pressure ratio propulsors," *Journal of Turbomachinery*, Vol. 137, No. 2, 2015. https://doi.org/10.1115/1.4028235.

[6] Rodert, L. A., and Garrett, F. B., "Ingestion of foreign objects into turbine engines by vortices," Tech. rep., 1955.

[7] Murphy, J. P., and MacManus, D. G., "Inlet ground vortex aerodynamics under headwind conditions," *Aerospace Science and Technology*, Vol. 15, No. 3, 2011, pp. 207–215. https://doi.org/10.1016/j.ast.2010.12.005, URL http://dx.doi.org/10.1016/j.ast.2010.12.005.

[8] Coschignano, A., and Babinsky, H., "Boundary-Layer Development Downstream of Normal Shock in Transonic Intakes at Incidence," *AIAA Journal*, Vol. 57, No. 12, 2019, pp. 5241–5251. https://doi.org/10.2514/1.j058508, URL https://doi.org/10.2514/1.J058508.

[9] Awes, A., Brosse, A., Dufour, G., Carbonneau, X., and Godard, B., "Effect of a vortex distortion on the operability of an ultra high bypass ratio fan," *Proceedings of the ASME Turbo Expo*, Vol. 2A-2020, 2020, pp. 1–11. https://doi.org/10.1115/GT2020-14596.

[10] Wakelam, C. T., Hynes, T. P., Hodson, H. P., Evans, S. W., and Chanez, P., "Separation control for aeroengine intakes, Part 1: Low-speed investigation of control strategies," *Journal of Propulsion and Power*, Vol. 28, No. 4, 2012, pp. 758–765. https://doi.org/10.2514/1.B34326, URL https://doi.org/10.2514/1.B34326.

[11] Wakelam, C. T., Hynes, T. P., Hodson, H. P., Evans, S. W., and Chanez, P., "Separation control for aeroengine intakes, Part 2: High-speed investigations," *Journal of Propulsion and Power*, Vol. 28, No. 4, 2012, pp. 766–772. https://doi.org/10.2514/1.B34327, URL https://doi.org/10.2514/1.B34327.

[12] Yeung, A., Vadlamani, N. R., Hynes, T., and Sarvankar, S., "Quasi 3D nacelle design to simulate crosswind flows: Merits and challenges," *International Journal of Turbomachinery, Propulsion and Power*, Vol. 4, No. 3, 2019, pp. 1–14. https://doi.org/10.3390/ijtpp4030025.

[13] Nichols, D. A., Vukasinovic, B., Glezer, A., Defore, M., Rafferty, B., and Palacios, F. D., "Characterization and control of nacelle inlet flow in crosswind," *AIAA Aviation 2019 Forum*, , No. June, 2019, pp. 1–16. https://doi.org/10.2514/6.2019-3685.

[14] Nichols, D. A., Vukasinovic, B., Glezer, A., Defore, M., and Rafferty, B., "Fluidic control of nacelle inlet flow in crosswind," *Aiaa Aviation 2020 Forum*, Vol. 1 PartF, 2020, pp. 1–15. https://doi.org/10.2514/6.2020-2955.

[15] Magrini, A., and Benini, E., "Study of geometric parameters for the design of short intakes with fan modelling," *Chinese Journal of Aeronautics*, Vol. 35, No. 11, 2022, pp. 18–32.

[16] Magrini, A., Bousi, D., and Benini, E., "Analysis of Ultra-High Bypass Ratio Turbofan Nacelle Geometries With Conventional and Short Intakes at Take-Off and Cruise," Vol. Volume 10C, 2022, p. V10CT33A005. https://doi.org/10.1115/GT2022-81912.

[17] Gunn, E. J., Brandvik, T., and Wilson, M. J., "Fan-Intake Coupling With Conventional and Short Intakes," *Turbo Expo: Power for Land, Sea, and Air*, Vol. Volume 1: Aircraft Engine; Fans and Blowers; Marine; Wind Energy; Scholar Lecture, 2021. https://doi.org/10.1115/GT2021-58829, URL https://doi.org/10.1115/GT2021-58829, v001T01A003.

[18] Silva, V. T., Lundbladh, A., Petit, O., and Xisto, C., "Multipoint aerodynamic design of ultrashort nacelles for ultrahigh-bypass-ratio engines," *Journal of Propulsion and Power*, Vol. 38, No. 4, 2022, pp. 541–558. https://doi.org/10.2514/1.B38497.

[19] Zantopp, S., MacManus, D., and Murphy, J., "Computational and experimental study of intake ground vortices," *The Aeronautical Journal*, Vol. 114, No. 1162, 2010, pp. 769–784.

[20] Mishra, N., MacManus, D., and Murphy, J., "Intake ground vortex characteristics," *Proceedings of the Institution of Mechanical Engineers, Part G: Journal of Aerospace Engineering*, Vol. 226, No. 11, 2012, pp. 1387–1400.

[21] Motycka, D. L., Walter, W., and Muller, G., "An analytical and experimental study of inlet ground vortices," *AIAA/SAE 9th Propulsion Conference*, , No. 73-1313, 1973. https://doi.org/10.2514/6.1973-1313.

[22] Freeman, C., and Rowe, A. L., "Intake Engine Interactions of a Modern Large Turbofan Engine," *Turbo Expo: Power for Land, Sea, and Air*, , No. 99-GT-344, 1999. https://doi.org/10.1115/99-GT-344.

[23] Lee, K.-B., Wilson, M., and Vahdati, M., "Effects of Inlet Disturbances on Fan Stability," *Journal of Engineering for Gas Turbines and Power*, Vol. 141, No. 5, 2019. https://doi.org/10.1115/1.4042204.

[24] Vadlamani, N. R., Cao, T., Watson, R., and Tucker, P. G., "Toward future installations: Mutual interactions of short intakes with modern high bypass fans," *Journal of Turbomachinery*, Vol. 141, No. 8, 2019, pp. 1–11. https://doi.org/10.1115/1.4044080.

[25] Boscagli, L., Christie, R., MacManus, D., and Piovesan, T., "Aerodynamics of a short intake in crosswind," *Aerospace Science and Technology*, Vol. 129, 2022, p. 107826. https://doi.org/https://doi.org/10.1016/j.ast.2022.107826.

[26] Mohankumar, B., Hall, C. A., and Wilson, M. J., "Fan aerodynamics with a short intake at high angle of attack," *Journal of Turbomachinery*, Vol. 143, No. 5, 2021, pp. 1–10. https://doi.org/10.1115/1.4050606.

[27] Moinier, P., "Algorithm developments for an unstructured viscous flow solver," Phd thesis, Oxford University, 1999.

[28] Almendral-Fernandez, G., Amirante, D., and Hills, N. J., "Use of a zonal hybrid URANS-LES methodology for prediction of rim seal ingestion into a low pressure turbine cavity," *2018 Joint Propulsion Conference*, 2018. https://doi.org/10.2514/6.2018-4917.

[29] Spalart, P. R., and Allmaras, S. R., "One-equation turbulence model for aerodynamic flows," *Recherche aerospatiale*, , No. 1, 1994, pp. 5–21. https://doi.org/10.2514/6.1992-439.

[30] Colin, Y., Aupoix, B., Boussuge, J., and Chanez, P., "Numerical Simulation of the Distortion Generated by Crosswind Inlet Flows," *Isabe-2007-1210*, 2007, pp. 1–13.

[31] Cao, T., Hield, P., and Tucker, P. G., "Hierarchical immersed boundary method with smeared geometry," *Journal of Propulsion and Power*, Vol. 33, No. 5, 2017, pp. 1151–1163. https://doi.org/10.2514/1.B36190.

[32] Cui, J., Watson, R., Ma, Y., and Tucker, P., "Low order modeling for fan and outlet guide vanes in aero-engines," *Journal of Turbomachinery*, Vol. 141, No. 3, 2019, pp. 1–9. https://doi.org/10.1115/1.4042202.

[33] Cao, T., Vadlamani, N. R., Tucker, P. G., Smith, A. R., Slaby, M., and Sheaf, C. T., "Fan-Intake interaction under high incidence," *Journal of Engineering for Gas Turbines and Power*, Vol. 139, No. 4, 2017, pp. 1–10. https://doi.org/10.1115/1.4034701.

[34] Carnevale, M., Wang, F., Green, J. S., and Mare, L. D., "Lip Stall Suppression in Powered Intakes," *Journal of Propulsion and Power*, Vol. 32, No. 1, 2016, pp. 161–170. https://doi.org/10.2514/1.B35811, URL https://doi.org/10.2514/1.B35811.

[35] Carnevale, M., Wang, F., and Mare, L. D., "Low Frequency Distortion in Civil Aero-engine Intake," *Journal of Engineering for Gas Turbines and Power*, Vol. 139, No. 4, 2017. https://doi.org/10.1115/1.4034600.

[36] Ma, Y., "Mixed-fidelity CFD Simulations for Aero-engines," Ph.D. thesis, University of Cambridge, 2019.

[37] CFD, I., "ANSYS ICEM CFD User's Manual," 2016.

[38] Milli, A., and Shahpar, S., "Padram: Parametric design and rapid meshing system for complex turbomachinery configurations," *Proceedings of the ASME Turbo Expo*, Vol. 8, No. PARTS A, B, AND C, 2012, pp. 2135–2148. https://doi.org/10.1115/GT2012-69030.

[39] Christie, R., Heidebrecht, A., and MacManus, D., "An automated approach to nacelle parameterization using intuitive class shape transformation curves," *Journal of Engineering for Gas Turbines and Power*, Vol. 139, No. 6, 2017, pp. 1–9. https://doi.org/10.1115/1.4035283.

[40] Christie, R., Robinson, M., Tejero, F., and MacManus, D. G., "The use of hybrid intuitive class shape transformation curves in aerodynamic design," *Aerospace Science and Technology*, Vol. 95, 2019, p. 105473. https://doi.org/10.1016/j.ast.2019.105473, URL https://doi.org/10.1016/j.ast.2019.105473.

[41] Kulfan, B. M., "Universal parametric geometry representation method," *Journal of aircraft*, Vol. 45, No. 1, 2008, pp. 142–158.

[42] Schlichting, H., and Gersten, K., *Boundary-layer theory*, Springer Science & Business Media, 2003.

[43] Cooley, J. W., and Tukey, J. W., "An algorithm for the machine calculation of complex Fourier series," *Mathematics of computation*, Vol. 19, No. 90, 1965, pp. 297–301.

[44] MacManus, D. G., Chiereghin, N., Prieto, D. G., and Zachos, P., "Complex aeroengine intake ducts and dynamic distortion," *AIAA Journal*, Vol. 55, No. 7, 2017, pp. 2395–2409. https://doi.org/10.2514/1.J054905.

[45] Migliorini, M., Zachos, P. K., and MacManus, D. G., "Novel Method for Evaluating Intake Unsteady Flow Distortion," *Journal of Propulsion and Power*, 2021, pp. 1–13. https://doi.org/10.2514/1.b38127.

[46] Van Der Wall, B. G., and Richard, H., "Analysis methodology for 3C PIV data," *31st European Rotorcraft Forum*, Vol. 2005, 2005.

[47] Wu, M., and Martin, M. P., "Analysis of shock motion in shockwave and turbulent boundary layer interaction using direct numerical simulation data," *Journal of Fluid Mechanics*, Vol. 594, 2008, pp. 71–83.

[48] Cousins, W. T., "History, philosophy, physics, and future directions of aircraft propulsion system/inlet integration," *Turbo Expo: Power for Land, Sea, and Air*, Vol. 41677, 2004, pp. 305–320.

[49] Bruce, P. J., and Babinsky, H., "Unsteady shock wave dynamics," *Journal of Fluid Mechanics*, Vol. 603, 2008, pp. 463–473. https://doi.org/10.1017/S0022112008001195.

[50] Davidson, T. S., and Babinsky, H., "Influence of boundary-layer state on development downstream of normal shock interactions," *AIAA Journal*, Vol. 56, No. 6, 2018, pp. 2298–2307. https://doi.org/10.2514/1.J056567.

[51] Ewert, R., and Schröder, W., "On the simulation of trailing edge noise with a hybrid LES/APE method," *Journal of Sound and Vibration*, Vol. 270, No. 3, 2004, pp. 509–524. https://doi.org/https://doi.org/10.1016/j.jsv.2003.09.047, URL https://www.sciencedirect.com/science/article/pii/S0022460X03012070, 2002 I.M.A. Conference on Computational Aeroacoustics.

[52] Murphy, J. P., and MacManus, D. G., "Ground vortex aerodynamics under crosswind conditions," *Experiments in Fluids*, Vol. 50, No. 1, 2011, pp. 109–124. https://doi.org/10.1007/s00348-010-0902-4.

[53] Sureshkumar, P., Lee, K.-B., Puente, R., and Stapelfeldt, S., "Impact of the Spatial Arrangement of Inlet Distortions on Resonant Fan Response," *Proceedings of Global Power and Propulsion Society*, 2022. https://doi.org/10.33737/gpps22-tc-132.

[54] Rao, A. N., Sureshkumar, P., Stapelfeldt, S., Lad, B., Lee, K.-B., and Rico, R. P., "Unsteady analysis of aeroengine intake distortion mechanisms: Vortex dynamics in crosswind conditions," *Journal of Engineering for Gas Turbines and Power*, Vol. 144, No. 12, 2022, p. 121005.

[55] Berthelon, T., Dugeai, A., Langridge, J., and Thouverez, F., "Analysis of vortex ingestion impact on the dynamic response of the fan in resonance condition," *Turbo Expo: Power for Land, Sea, and Air*, Vol. 58684, American Society of Mechanical Engineers, 2019, p. V07AT36A010.

[56] Vahdati, M., Lee, K.-B., and Sureshkumar, P., "A Review of Computational Aeroelasticity Of Civil Fan Blades," *International Journal of Gas Turbine, Propulsion and Power Systems*, Vol. 11, No. 4, 2020, pp. 22–35.

[57] Pagès, V., Duquesne, P., Aubert, S., Blanc, L., Ferrand, P., Ottavy, X., and Brandstetter, C., "UHBR Open-Test-Case Fan ECL5/CATANA," *International Journal of Turbomachinery, Propulsion and Power*, Vol. 7, No. 2, 2022, p. 17.

2023-10-13

Effect of unsteady fan-intake interaction on short intake design

Boscagli, Luca

American Society of Mechanical Engineers

Boscagli L, MacManus DG, Christie R, Sheaf CTJ. (2023) Effect of unsteady fan-intake interaction on short intake design. Journal of Engineering for Gas Turbines and Power, Available online 13 October 202, Paper number GTP-23-1195

https://doi.org/10.1115/1.4063768